

國立交通大學

電子工程學系 電子研究所碩士班

碩 士 論 文

應用於數位電視廣播系統之低複雜度頻率同步化設計



**Low Complexity Carrier Frequency Synchronization
for DVB-T/H System**

學生：簡盧忠

指導教授：李鎮宜 教授

中華民國九十四年七月

應用於數位電視廣播系統之低複雜度頻率同步化設計

Low Complexity Carrier Frequency Synchronization
for DVB-T/H System

研究生：簡盧忠

Student : Lu-Chung Chien

指導教授：李鎮宜

Advisor : Chen-Yi Lee

國立交通大學
電子工程學系 電子研究所 碩士班
碩士論文



Submitted to Institute of Electronics
College of Electrical Engineering and Computer Science
National Chiao Tung University
in Partial Fulfillment of the Requirements
for the Degree of
Master of Science
in

Electronics Engineering

July 2005

Hsinchu, Taiwan, Republic of China

中華民國九十四年七月

應用於數位電視廣播系統之低複雜度頻率同步化設計


學生：簡盧忠

指導教授：李鎮宜 教授

國立交通大學

電子工程學系 電子研究所碩士班

摘要



在本論文中，我們提出了一個應用於數位電視廣播系統的低複雜度載波頻率同步化設計。此同步化設計由兩組偵測機制及一組追蹤迴路組成。與傳統的演算法相比，我們所提出的小數倍載波頻率漂移偵測機制可以有效的對抗多重路徑延遲造成的干擾，並且在均方根錯誤可達到 0.25~7.8 分貝的信號雜訊比改進。在整數倍載波頻率漂移偵測機制方面，我們所提出的二階段架構可以有效的減少偵測範圍以降低運算複雜度。此外，為了偵測正確的整數倍載波頻率漂移值，我們提出了兩種低複雜度的演算法，在不影響整體系統效能的前提下，相較於傳統的演算法可以減少超過 80% 以上的乘法次數。提出的三階段載波頻率漂移追蹤迴路亦可有效的降低殘留的誤差。利用我們所提出的低複雜度載波頻率同步化設計，對整體數位電視廣播系統平台而言，在嚴重的傳輸環境包括 Rayleigh 衰減通道、杜普勒頻率 70 赫茲、取樣頻率漂移百萬分之 20、載波頻率漂移百萬分之 92.14 情況下，載波頻率同步化誤差造成的訊號雜訊比損失仍小於 0.2 分貝。基於我們所提出的低複雜度載波頻率同步化設計，在 2005 年 6 月，我們使用 0.18 微米製程實現了數位電視廣播系統基頻接收器的晶片設計。

Low Complexity Carrier Frequency Synchronization for DVB-T/H System

Student : Lu-Chung Chien

Advisor : Dr. Chen-Yi Lee

Institute of Electronics Engineering

National Chiao Tung University

ABSTRACT

In this thesis, a low complexity carrier frequency offset (CFO) synchronization scheme is proposed for Digital Video Broadcasting-Terrestrial/Handheld (DVB-T/H) system, which comprises two acquisition strategies and a tracking loop. The proposed fractional CFO acquisition algorithm can overcome the distortion caused by multipath delay spread and achieves 0.25~7.8dB gain in RMSE compared with the conventional approach. A 2-stage scheme is proposed for the integral CFO acquisition to reduce the search range. Besides, two low complexity algorithms are also proposed to detect the accurate integral CFO value and save more than 80% of number of multiplication without any performance loss to the overall system compared with the conventional approach. The proposed three stage CFO tracking loop can reduce the residual CFO error effectively. The SNR loss due to the proposed CFO synchronization scheme of the overall DVB-T/H baseband receiver system is less than 0.2dB even in severe channel distortion including Rayleigh channel, Doppler spread 70Hz, CFO 92.14ppm (10.33 subcarrier spacing) and sampling clock offset 20ppm. Based on the proposed low complexity CFO synchronization scheme, a DVB-T/H baseband receiver is implemented with 0.18 μ m cell library and tapped out in Jun. 2005.

誌 謝

從大三做專題以來，Si2 這個大家庭已經與我共度了三年多的時光。在這裡不但學到了許多專業知識，為人處事方面更是受益良多。

能完成這本論文，我最感謝的，是 李鎮宜教授這三年多以來不厭其煩的指導與研究方向的指引，讓我在研究遇到挫折或困難時，得以重新找到突破瓶頸的方法。此外，也要感謝 李鎮宜教授為實驗室提供完善的研究設備，使我的研究得以順利完成。

在這裡，也要特別感謝 DVB group 的黎峰學長、昱偉學長、陳元學長、成偉學長、英豪以及家豪兩位學弟，感謝大家這兩年來的腦力激盪與相互討論，不但使我在相關的研究領域有所精進，更學習到團隊合作的可貴。

還要感謝與我同屆的亭安、勝仁、凱立、林宏與瑋哲，在這兩年內，我們一起經歷過許多風風雨雨，有歡笑也有淚水，有你們的陪伴，使我這兩年的碩士生涯充滿了多彩多姿的回憶。

最後，我要由衷的感謝我的父母及家人，感謝你們多年來的栽培及細心，讓我能順利完成碩士的學業。更要感謝我的女友舒慧，這幾年來有妳的一路相伴，使我的生活不再孤單，更期待未來的日子裡，能與妳度過人生的旅程。僅將此論文獻給你們，以表達我最深的感激。

Contents

CHAPTER 1 . INTRODUCTION.....	1
1.1 MOTIVATION.....	1
1.2 INTRODUCTION TO DVB-T/H SYSTEM.....	2
1.3 ORGANIZATION OF THIS THESIS.....	7
CHAPTER 2 . CARRIER FREQUENCY OFFSET SYNCHRONIZATION	
ALGORITHMS	8
2.1 INTRODUCTION TO CARRIER FREQUENCY OFFSET	8
2.1.1 <i>Signal Model of Carrier Frequency Offset.....</i>	<i>9</i>
2.1.2 <i>Effect of Carrier Frequency Offset.....</i>	<i>10</i>
2.2 CARRIER FREQUENCY OFFSET SYNCHRONIZATION SCHEME.....	12
2.3 FRACTIONAL CARRIER FREQUENCY OFFSET SYNCHRONIZATION.....	14
2.4 INTEGRAL CARRIER FREQUENCY OFFSET SYNCHRONIZATION	17
2.4.1 <i>Conventional Pilots Based Approach.....</i>	<i>17</i>
2.4.2 <i>Conventional Guard Band Based Approach.....</i>	<i>20</i>
2.4.3 <i>Proposed 2-stage Approach.....</i>	<i>22</i>
2.4.4 <i>The First Stage of the Proposed Approach.....</i>	<i>23</i>
2.4.5 <i>The Second Stage of the Proposed Approach</i>	<i>24</i>
2.5 RESIDUAL CARRIER FREQUENCY OFFSET SYNCHRONIZATION	27
2.5.1 <i>Residual CFO Estimation.....</i>	<i>28</i>
2.5.2 <i>Residual CFO Tracking Loop Filter.....</i>	<i>31</i>
CHAPTER 3 . SIMULATION AND PERFORMANCE ANALYSIS	33

3.1	SIMULATION PLATFORM.....	33
3.2	CHANNEL MODEL.....	36
3.2.1	<i>Multipath Fading Channel Model</i>	37
3.2.2	<i>Doppler Spread Model</i>	39
3.2.3	<i>Carrier Frequency Offset and Sampling Clock Offset model</i>	40
3.3	PERFORMANCE ANALYSIS.....	41
3.3.1	<i>Fractional Carrier Frequency Offset Synchronization</i>	42
3.3.2	<i>Integral Carrier Frequency Offset Synchronization</i>	46
3.3.3	<i>Residual Carrier Frequency Offset Tracking</i>	55
3.3.4	<i>Overall System Performance</i>	58
CHAPTER 4. ARCHITECTURE AND IMPLEMENTATION.....		62
4.1	DESIGN METHODOLOGY.....	62
4.2	ARCHITECTURE OF THE DVB-T/H BASEBAND RECEIVER.....	63
4.3	ARCHITECTURE OF CARRIER FREQUENCY OFFSET SYNCHRONIZATION.....	66
4.3.1	<i>Fractional Carrier Frequency Offset Synchronization</i>	66
4.3.2	<i>Integral Carrier Frequency Offset Synchronization</i>	67
4.3.3	<i>Residual Carrier Frequency Offset Tracking</i>	69
4.4	DVB-T/H BASEBAND RECEIVER CHIP SUMMARY.....	70
CHAPTER 5. CONCLUSION AND FUTURE WORK.....		72
BIBLIOGRAPHY.....		73

List of Figures

FIG. 1.1 FUNCTIONAL BLOCK DIAGRAM OF DVB-T SYSTEM	3
FIG. 1.2 BLOCK DIAGRAM OF DVB-H CODEC AND TRANSMITTER	5
FIG. 2.1 SPECTRUM OF FIVE ORTHOGONAL SUBCARRIERS OF OFDM SYSTEMS.....	8
FIG. 2.2 PHASE ROTATION IN TIME DOMAIN FOR LONG TIME RECEPTION WHEN $\epsilon=0.01$	11
FIG. 2.3 SPECTRUM OF FIVE SUBCARRIERS IN CARRIER FREQUENCY OFFSET ENVIRONMENT	11
FIG. 2.4 OVERALL CFO SYNCHRONIZATION AND COMPENSATION SCHEME.....	13
FIG. 2.5 GUARD INTERVAL INSERTION AND MULTIPATH CHANNEL SPREAD.....	15
FIG. 2.6 RECEIVED SIGNAL IN FREQUENCY DOMAIN WHEN CFO=1 SUBCARRIER SPACE.....	18
FIG. 2.7 RECEIVED SYMBOL IN FREQUENCY DOMAIN WHEN CFO IS -2.....	21
FIG. 2.8 PROPOSED 2-STAGE INTEGRAL CFO ALGORITHM SCHEME.....	22
FIG. 2.9 THE FIRST STAGE OF THE PROPOSED INTEGRAL CFO ESTIMATOR.....	23
FIG. 2.10 THE PROPOSED GUARD BAND POWER DETECTION BASED APPROACH	27
FIG. 2.11 THE TRACKING LOOP OF THE CFO SYNCHRONIZATION	28
FIG. 2.12 PHASE ROTATION BETWEEN TWO SUCCESSIVE OFDM SYMBOLS	30
FIG. 2.13 BLOCK DIAGRAM OF PI LOOP FILTER	32
FIG. 3.1 OVERALL DVB-T/H PLATFORM	33
FIG. 3.2 THE BASEBAND RECEIVER DESIGN.....	35
FIG. 3.3 FUNCTIONAL BLOCKS OF INNER RECEIVER.....	36
FIG. 3.4 CHANNEL MODEL OF DVB-T/H SYSTEM	37
FIG. 3.5 CHANNEL RESPONSE OF RAYLEIGH AND RICEAN ($K=10\text{dB}$) CHANNEL	39
FIG. 3.6 DOPPLER SPREAD MODEL	39
FIG. 3.7 BER PERFORMANCE IN DIFFERENT CFO ERROR.....	41

FIG. 3.8 RMSE PERFORMANCE IN DIFFERENT GUARD INTERVAL LENGTH	43
FIG. 3.9 RMSE PERFORMANCE IN DIFFERENT γ	44
FIG. 3.10 RMSE PERFORMANCE COMPARISON	45
FIG. 3.11 PERFORMANCE OF THE FIRST STAGE WITH DIFFERENT WINDOW WIDTH.....	47
FIG. 3.12 PERFORMANCE OF THE FIRST STAGE IN DIFFERENT CHANNEL MODELS.....	48
FIG. 3.13 CONTINUAL PILOTS BASED APPROACH WITH DIFFERENT NUMBER OF PILOTS	49
FIG. 3.14 PROPOSED GUARD BAND BASED APPROACH WITH DIFFERENT WINDOW WIDTH	50
FIG. 3.15 PERFORMANCE OF DIFFERENT INTEGRAL CFO ESTIMATORS IN GAUSSIAN CHANNEL .	51
FIG. 3.16 PERFORMANCE OF DIFFERENT INTEGRAL CFO ESTIMATORS IN RICEAN CHANNEL.....	52
FIG. 3.17 PERFORMANCE OF DIFFERENT INTEGRAL CFO ESTIMATORS IN STATIC RAYLEIGH CHANNEL	53
FIG. 3.18 PERFORMANCE OF DIFFERENT INTEGRAL CFO ESTIMATORS IN MOBILE RAYLEIGH CHANNEL	54
FIG. 3.19 RMSE OF ONE-SHOT RESIDUAL CFO ESTIMATOR IN DIFFERENT CHANNEL MODELS ...	56
FIG. 3.20 CFO TRACKING LOOP IN WITH DIFFERENT PARAMETERS.....	57
FIG. 3.21 RESIDUAL CFO TRACKING LOOP WITH DIFFERENT STAGE.....	58
FIG. 3.22 OVERALL SYSTEM PERFORMANCE IN GAUSSIAN CHANNEL.....	59
FIG. 3.23 OVERALL SYSTEM PERFORMANCE IN RICEAN CHANNEL	60
FIG. 3.24 OVERALL SYSTEM PERFORMANCE IN RAYLEIGH CHANNEL	60
FIG. 3.25 OVERALL SYSTEM PERFORMANCE IN MOBILE RAYLEIGH CHANNEL	61
FIG. 4.1 PLATFORM-BASED DESIGN METHODOLOGY	63
FIG. 4.2 ARCHITECTURE OF THE DVB-T/H BASEBAND RECEIVER	65
FIG. 4.3 ARCHITECTURE OF FRACTIONAL CFO ESTIMATOR.....	66
FIG. 4.4 ARCHITECTURE OF THE FIRST STAGE OF THE PROPOSED INTEGRAL CFO ESTIMATOR	68
FIG. 4.5 ARCHITECTURE OF THE SECOND STAGE OF THE PROPOSED INTEGRAL CFO ESTIMATOR	68
FIG. 4.6 ARCHITECTURE OF THE JOINT RESIDUAL CFO/SCO ESTIMATOR.....	69



List of Tables

TABLE 1-1 PARAMETERS FOR 8MHZ CHANNEL IN DVB-T STANDARD.....	4
TABLE 1-2 PARAMETERS FOR 8MHZ CHANNEL IN DVB-H STANDARD.....	6
TABLE 3-1 PERFORMANCE COMPARISON OF FRACTIONAL CFO ESTIMATOR.....	45
TABLE 3-2 PARAMETERS OF THE PROPOSED INTEGRAL CFO ESTIMATOR.....	50
TABLE 3-3 NUMBER OF MULTIPLICATION COMPARISON.....	55
TABLE 3-4 SNR LOSS DUE TO SYNCHRONIZATION IN DIFFERENT CHANNEL MODELS.....	61
TABLE 4-1 SYNTHESIS RESULT OF THE FRACTIONAL CFO ESTIMATOR.....	67
TABLE 4-2 SYNTHESIS RESULT OF THE INTEGRAL CFO ESTIMATOR.....	69
TABLE 4-3 SYNTHESIS RESULT OF THE RESIDUAL CFO TRACKING SCHEME.....	70
TABLE 4-4 CHIP FEATURE.....	70



Chapter 1 .

Introduction

In this chapter, we will describe the motivation of this research first. Introduction to the DVB-T/H standard will be made later. Finally, the organization of this thesis will be listed in the end of this chapter.

1.1 Motivation

Orthogonal frequency division multiplexing (OFDM) is a multicarrier transmission technique which uses parallel data transmission and frequency division multiplexing and was drawn firstly in 1960s [1-2]. Because of the high channel efficiency, OFDM is widely applied in the new generation wireless access systems such as digital broadcasting systems [3-4] and wireless local area network (WLAN) [5-6]. The technique of using orthogonal subcarriers saves the bandwidth, but increases the sensitivity to synchronization errors. Therefore, synchronization plays a very important role in OFDM based systems.

Due to the orthogonality between subcarriers, OFDM is very sensitive to the carrier frequency offset (CFO) induced by the mismatch of oscillator frequency between transmitter and receiver. Once CFO exists, the orthogonality of subcarriers will be destroyed and the system performance will be degraded because of inter-carrier interference (ICI) noise. Hence carrier frequency synchronization is very important for OFDM systems.

The objective of this thesis is to design a low complexity CFO synchronization scheme which estimates and tracks the CFO fast and precisely. The complete CFO synchronization scheme is composed of acquisition stage and tracking stage, where the former can be divided

into fractional acquisition and integral acquisition, respectively. In this thesis, we choose Digital Video Broadcasting-Terrestrial/Handheld (DVB-T/H) as the research topic because DVB-T/H is a narrow subcarrier spacing and continuous time reception OFDM system. These features will increase the difficulty of CFO synchronization. A low complexity CFO synchronization scheme for DVB-T/H system will be proposed in this thesis.

1.2 Introduction to DVB-T/H system

Digital Video Broadcasting-Terrestrial (DVB-T) has been subjected to technical discussion for many years and undoubtedly been shown as a great success in delivering high quality digital television by terrestrial means [3]. DVB-T standard has been produced by European Telecommunication Standard Institute (ETSI) in Aug, 1997. It has been applied in many countries around the world such as Taiwan. Although the DVB-T reception can be applied in mobile environment, the ability of reception for handheld terminals is still not good enough because of its high operation power. Therefore, Digital Video Broadcasting-Handheld (DVB-H) was also proposed based on the DVB-T technology to provide broadcast services for handheld devices such as PDAs or mobile phones [7]. The detailed concepts of DVB-T and DVB-H will be illustrated later.

The transmission system of the DVB-T standard is shown in Fig. 1.1. It contains the blocks for source coding, outer coding and interleaving, inner coding and interleaving, mapping, OFDM modulation, and frame adaptation, respectively. In the case of two-level hierarchy, the functional block diagram of the system must be expended to include the modules shown in dashed line. As we can see the source coding of audio and video signals is based on ISO-MPEG2 standard. After the MPEG2 transport multiplexer, a Reed-Solomon (RS) shortened code (204,188, $t=8$) and a convolutional byte-wise interleaving with depth $I=12$ shall be applied to generate error protected packets. As Fig. 1.1 shows, the outer

interleaver is followed by the inner coder. This coder is designed for a range of punctured convolutional codes, which allows code rates of 1/2, 2/3, 3/4, 5/6, and 7/8. If two-level hierarchical transmission is used, each of two parallel inner codes has its own code rate. Afterward, the inner interleaver is block based bit-wise interleaving. The constellation mapping for OFDM subcarriers operates with various modes after the inner interleaver. The constellation modes are QPSK, 16-QAM, 64-QAM, non-uniform 16-QAM, and non-uniform 64-QAM, respectively. The transmission channel bandwidth is 6MHz, 7MHz, and 8MHz, respectively.

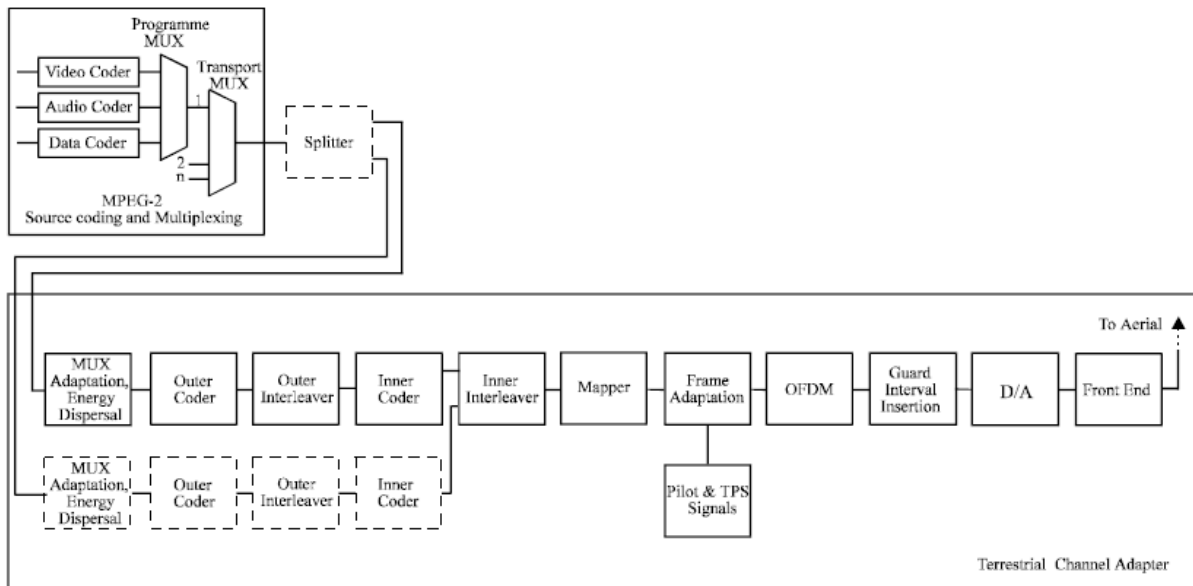


Fig. 1.1 Functional Block diagram of DVB-T system

The DVB-T system uses OFDM technique with various transmission parameters. The parameters for 8MHz channel bandwidth in DVB-T standard are listed in Table 1-1. Two modulation modes are defined: a 2k mode and an 8k mode. The 2k mode is suitable for short distance transmission and high speed mobile reception because of its short symbol duration and wide subcarrier spacing. On the contrary, the 8k mode is suitable for long distance transmission and deep multipath spread. Other parameters such as code rate, constellation mode, and guard interval length can also be decided properly according to the broadcasting channel condition of the local area.

Table 1-1 Parameters for 8MHz channel in DVB-T standard

Parameter	8k mode	2k mode
Number of subcarriers K	6817	1705
Value of carrier number K_{min}	0	0
Value of carrier number K_{max}	6816	1704
FFT size N	8192	2048
Symbol duration T_U	896 μ s	224 μ s
Subcarrier spacing $1/T_U$	1.116KHz	4.464KHz
Spacing between K_{min} and K_{max}	7.61MHz	7.61MHz
Guard interval N_g/N	1/4,1/8,1/16,1/32	1/4,1/8,1/16,1/32

An OFDM frame consists of 68 OFDM symbols and four frames constitute a super-frame. In addition to the transmitted data, an OFDM symbol contains several kinds of reference signals for synchronization and channel estimation such as scattered pilots, continual pilots, and TPS (Transmission Parameter Signaling) pilots. Scattered pilots are inserted every 12 subcarriers and have an interval of three subcarriers in the next adjacent symbol. Continual pilots locate at fixed subcarrier index which contain 177 for 8k mode and 45 for 2k mode, respectively. Both scattered pilots and continual pilots are transmitted at boosted power level of 16/9 whereas the data subcarriers are normalized to 1, and modulated according to the PRBS (Pseudo Random Binary Sequence) sequence $(X^{11}+X^2+1)$. The TPS pilots are used for signaling parameters related to transmission scheme, i.e. to channel coding and modulation. The TPS pilots are defined over 68 consecutive OFDM symbols and transmitted in parallel on 17 TPS subcarriers for 2k mode and 68 for 8k mode. Each OFDM symbol conveys one TPS bit which is differentially encoded in every TPS subcarrier. The TPS information contains frame number, constellation, hierarchy, code rate, guard interval, FFT mode, and BCH error protection code, respectively. Unlike continual and scattered pilots, TPS

pilots are transmitted as the normal power level of 1 with DBPSK modulation.

The DVB-H technology is a spin-off of the DVB-T standard. It is large extent compatible to DVB-T but takes into account the specific properties of the addressed terminals- small, lightweight, portable, battery-powered devices in mobile environment. Unlike the DVB-T transport stream adopted from the MPEG2 standard, the DVB-H system is IP (Internet Protocol)-based, therefore the outer DVB-H interface is the IP interface. The IP data are embedded into the transport stream by means of the MPE (Multi Protocol Encapsulation) frame, an adaptation protocol defined in the DVB Data Broadcasting Specification [8]. One MPE frame contains one or more IP datagrams and has a maximum number of 1024 rows and a constant number of 255 columns. The block diagram of DVB-H codec and transmitter is as shown in Fig. 1.2.

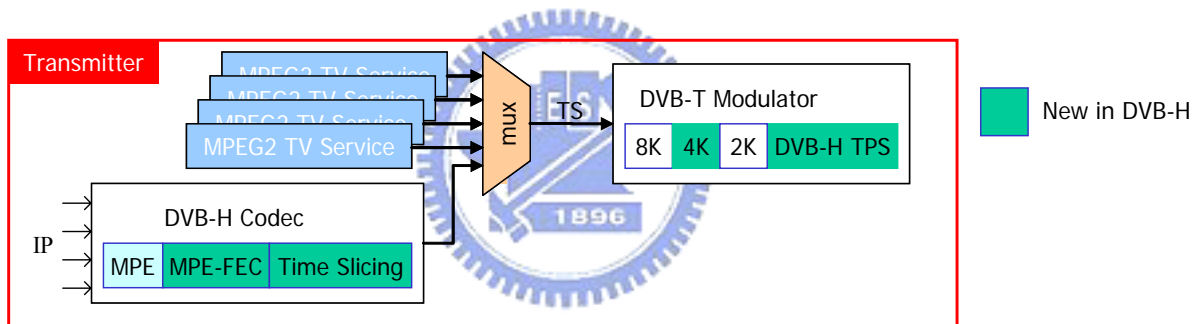


Fig. 1.2 Block diagram of DVB-H codec and transmitter

As we can see the DVB-H codec is composed of the MPE, MPE-FEC, and time slicing. In order to satisfy the low power issue in battery-powered terminals, a time-multiplexed transmission of different service is exploited. This technique, called time slicing, allows for selective access to desired data and results in a large battery power saving effect. The burst duration of time slicing is in the range of several hundred ms whereas the off-time may amount to several seconds. The lead time for power-on and resynchronization is assumed to be less than 250ms. Depending on the duty/turn-off ratio, the resulting power saving may be more than 90%. For mobile channels reception and long delay spread conditions, an enhanced error protection scheme on the link layer is needed. This scheme is called MPE-FEC and

employs powerful channel coding and time interleaving. The MPE-FEC scheme consists of an RS code in conjunction with an extensive block interleaving. The RS (255, 191, 64) code is utilized to perform MPE-FEC error protection. Besides, a virtual block interleaving effect is also performed by reading from and writing to the MPE frame in column direction whereas coding is applied in row direction.

As for the physical layer, the DVB-H is compatible with the DVB-T standard except some additional points. First, the DVB-H provides new TPS pilots which exploit the reserved TPS subcarriers defined in the DVB-T standard. The new contents of the TPS pilots provide the information about MPE-FEC and time slicing. Besides, an additional OFDM transmission mode and a new symbol interleaving method within the inner interleaver, 4k mode and in-depth interleaving, are also provided by the new TPS pilots. DVB-H provides an intermediate 4k mode with 4096-point FFT in the OFDM modulation. The 4k mode represents a compromise solution between the 2k and 8k mode to satisfy long distance transmission and mobile reception. The in-depth interleaving allows the symbol interleaver operates at 8k interleaving length while the 2k or 4k mode is applied to improve the interleaving performance. Besides, the DVB-H also supports 5MHz transmission channel bandwidth. The parameters for 8MHz channel bandwidth in DVB-H standard are listed in Table 1-2.

Table 1-2 Parameters for 8MHz channel in DVB-H standard

Parameter	8k mode	4k mode	2k mode
Number of subcarriers K	6817	3409	1705
Value of carrier number K_{min}	0	0	0
Value of carrier number K_{max}	6816	3408	1704
FFT size N	8192	4096	2048
Symbol duration T_U	896 μ s	448 μ s	224 μ s

Subcarrier spacing $1/T_U$	1.116KHz	2.232KHz	4.464KHz
Spacing between K_{min} and K_{max}	7.61MHz	7.61MHz	7.61MHz
Guard interval N_g/N	1/4,1/8,1/16,1/32	1/4,1/8,1/16,1/32	1/4,1/8,1/16,1/32

1.3 Organization of This Thesis

This thesis is organized as follows. In chapter 2, the signal models and the detailed algorithms of the proposed CFO synchronization scheme will be introduced. The simulation result and performance analysis will be discussed in chapter 3. Chapter 4 will introduce the design methodology, hardware architecture, and the chip summary of the proposed design. Conclusion and future work will be given in chapter 5.



Chapter 2 .

Carrier Frequency Offset Synchronization Algorithms

In this chapter, we introduce the signal model and the effect of carrier frequency offset (CFO) in DVB-T/H system first. The algorithms of CFO synchronization in different synchronization categories will be illustrated in later sections. Some comparison and discussion between developed and the proposed algorithms are also made.

2.1 Introduction to Carrier Frequency Offset

OFDM is a bandwidth efficient signal scheme for digital communications. In OFDM systems, the spectrum of the individual subcarrier mutually overlaps and exhibits orthogonality to achieve optimum spectrum efficiency as shown in Fig. 2.1.

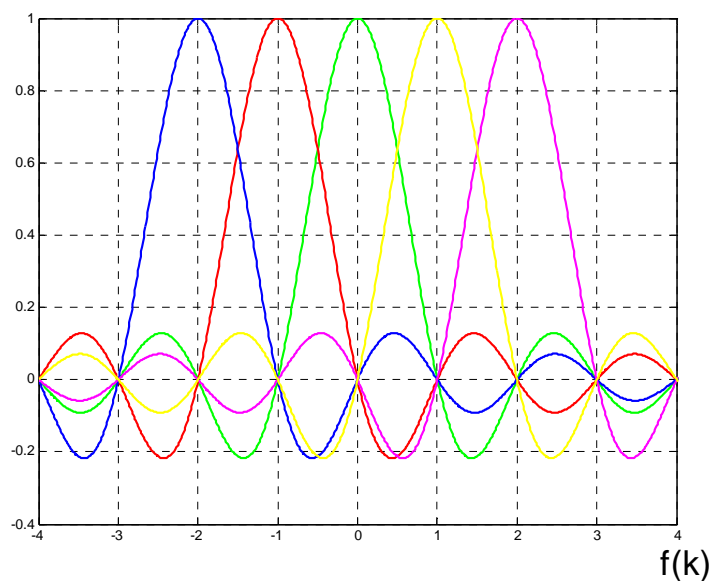


Fig. 2.1 Spectrum of five orthogonal subcarriers of OFDM systems

However, OFDM is very sensitive to the CFO introduced by the mismatch of oscillator frequency between transmitter and receiver. CFO causes linear phase error in time domain and shifts the subcarrier index in frequency domain, respectively. Once CFO exists, the orthogonality between subcarriers will be destroyed and the degradation of the system performance will be serious. Compared with other OFDM based system such as IEEE 802.11a, the subcarrier space of DVB-T/H system is relatively narrower and the tolerance of carrier frequency offset is also worse [3][5]. Hence the CFO synchronization is a very critical problem to be solved in DVB-T/H system.

2.1.1 Signal Model of Carrier Frequency Offset

Consider an OFDM system using an inverse fast Fourier transform (IFFT) of size N for modulation. Each OFDM symbol is composed of K ($K < N$) data subcarriers $a_{l,k}$, where l denotes the OFDM symbol index and k ($0 \leq k < K$) denotes the subcarrier index. After IFFT, a cyclic prefix composed of N_g samples is inserted to avoid the influence of multipath channel delay spread. So a transmitted symbol has $N_s = N + N_g$ samples with sample period T . The transmitted complex baseband signal of the l -th symbol can be expressed as

$$s_l(t) = e^{j2\pi f_{c,tx} t} \left\{ \frac{1}{N} \sum_{k=0}^{K-1} a_{l,k} \cdot e^{\frac{j2\pi k'(t - (N_g + l \cdot N_s)T)}{NT}} \right\} \quad (2-1)$$

where $f_{c,tx}$ is the central frequency of the transmitter RF oscillator, and k' is the subcarrier index relative to the centre frequency, $k' = k - (K - 1)/2$.

Since the CFO Δf ($\Delta f = f_{c,tx} - f_{c,rx}$) between transmitter and receiver RF oscillator can be expressed as a time-variant phase error, $e^{j2\pi\Delta f t}$, the l -th received symbol after sampling with period T' at time instants $t_n = (lN_s + N_g + n)T'$ and removing guard interval can be expressed as

$$\begin{aligned}
r_l(n) &= e^{j2\pi\Delta f t_n} \cdot s_l(t_n) * h(t_n, \tau) + w_l(n) \\
&= e^{j2\pi\Delta f t_n} \cdot \frac{1}{N} \sum_{k=0}^{K-1} a_{l,k} \cdot e^{\frac{j2\pi k(t_n - (N_g + l \cdot N_s)T)}{NT}} * h(t_n, \tau) + w_l(n) \quad (2-2)
\end{aligned}$$

where $h(t_n, \tau)$ is the channel impulse response with delay spread τ , $w_l(n)$ is the complex-valued additive white Gaussian noise (AWGN). After demodulation via a fast Fourier transform (FFT), the l -th OFDM symbol at subcarrier k , $R_{l,k}$ is as follows

$$\begin{aligned}
R_{l,k} &= \sum_{n=0}^{N-1} r_l(n) e^{-j2\pi k' n / N} \\
&= e^{j2\pi\epsilon (lN_s + N_g)(1+\zeta) / N} e^{j\frac{2\pi k'}{N} (lN_s + N_g)\zeta} \cdot \alpha \cdot H_{l,k} \cdot a_{l,k} + ICI_{l,k} + W_{l,k} \quad (2-3)
\end{aligned}$$

where $\epsilon = \Delta f NT$ is the CFO value normalized with the subcarrier space, ζ is the sampling clock offset (SCO) ($\zeta = (T' - T) / T$), α is an attenuation factor which is close to 1, and $ICI_{l,k}$ is the inter-carrier interference noise due to carrier frequency offset. Likewise, $H_{l,k}$ is the channel frequency response on the k -th subcarrier of the l -th OFDM symbol with the assumption that the channel is stationary within at last one symbol, $W_{l,k}$ is a zero-mean stationary complex process as well.

2.1.2 Effect of Carrier Frequency Offset

As previous section shows, CFO introduces various imperfect effects to the received signal. From the viewpoint of time domain, the CFO can be expressed as a time-variant phase error. The rotated phase error is in proportion to the received sample time instants t_n and can be expressed as

$$\theta_l(n) = 2\pi\Delta f t_n = 2\pi\epsilon (lN_s + N_g + n) / N \quad (2-4)$$

where θ is the phase rotation caused by CFO. Unlike other packet-based communication systems such as IEEE 802.11a, DVB-T/H is a continuous-data transmission system and the

receiving of data continues until the receiver is turned off. So the phase error will still be large even in very weak CFO environment when the receiver operates for a long time as shown in Fig. 2.2.

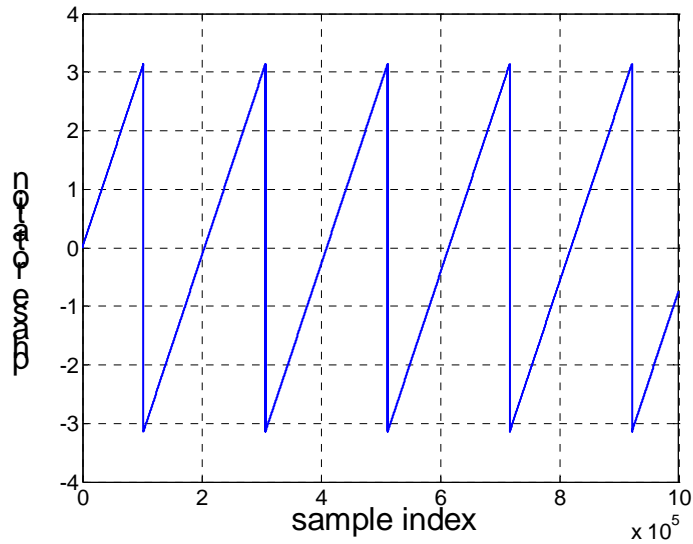


Fig. 2.2 Phase rotation in time domain for long time reception when $\epsilon=0.01$

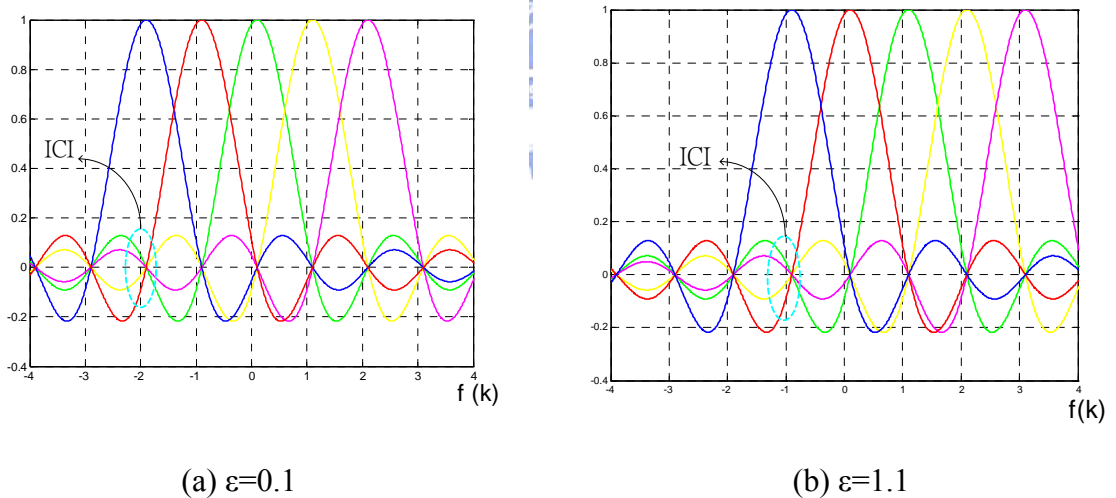


Fig. 2.3 Spectrum of five subcarriers in carrier frequency offset environment

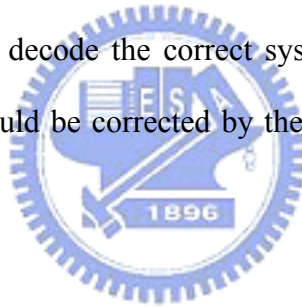
CFO results in different effects in frequency domain. It not only reduces the amplitude but also shifts the phase of the demodulated signal. Further more, the second term of (2-3) $ICI_{l,k}$ degrades the system performance strongly because it destroys the orthogonality within each subcarrier in OFDM symbols, and can be expressed as

$$ICI_{l,k} = \sum_{\substack{\tilde{k}=0 \\ \tilde{k} \neq k}}^{K-1} H_{l,k} a_{l,k} \frac{\sin(\pi\varepsilon)}{N \sin(\pi(\tilde{k}-k+\varepsilon)/N)} \cdot e^{j\pi\varepsilon(N-1)/N} e^{-j\pi(\tilde{k}-k)/N} . \quad (2-5)$$

Because the subcarrier space of DVB-T/H system is very narrow (about 0.7~4.5 KHz), we can divide the normalized CFO value into integral part and fractional part, and can be expressed as

$$\varepsilon = \varepsilon_I + \varepsilon_F \quad (2-6)$$

From Fig. 2.3, we can find that CFO causes inter-carrier interference noise within each subcarrier and makes the orthogonality of spectrum lost. Once the integral part of CFO ε_I is not zero, all of the subcarriers will shift circularly. The shift of subcarrier index will make the channel estimator receive wrong pilot sequence at the pre-defined pilot index and then the calculated channel frequency response will be not reliable. Also the TPS decoder can not receive correct TPS pattern to decode the correct system parameter. All of these imperfect effects in different domain should be corrected by the aid of CFO synchronization to obtain good receiving performance.



2.2 Carrier Frequency Offset Synchronization Scheme

From previous section, we can know that the imperfect effects caused by CFO degrade the system performance enormously. Besides, the DVB-T/H system is very sensitive to the CFO because of its narrow subcarrier space and continuous-data transmission scheme. So the synchronization of CFO is a very important factor and must be handled carefully. In our system platform, the CFO synchronization is divided into acquisition stage and tracking stage. As the beginning of receiving data, the acquisition stage estimates the CFO value roughly with the first 3 received symbols. After acquisition stage finishes, the integral CFO value $\hat{\varepsilon}_I$ and most of the fractional CFO value $\hat{\varepsilon}_F$ should be estimated and compensated. The

tracking stage then turned on to track the residual fractional CFO value ε_R ($\varepsilon_F = \hat{\varepsilon}_F + \varepsilon_R$) left by the acquisition stage until the receiver is turned off.

The objective of CFO synchronization is to establish subcarrier orthogonality as fast and accurately as possible (acquisition) and then maintain orthogonality as well as possible at all times during online reception (tracking). However, a CFO acquisition algorithm alone can not be both fast and sufficiently accurate, because

1. Pre-FFT algorithms allow only fast acquisition of the fractional CFO but no acquisition of the integral CFO.
2. Post-FFT algorithms allow fast acquisition of the integral CFO but, due to lack of orthogonality, acquisition of fractional CFO is very complicate.

Both fast and accurate acquisition can be attained by adopting a multi-stage synchronization strategy with two one-shot acquisition stages (one pre-FFT and the other post-FFT) followed by tracking. In DVB-T/H system, the data format provides for training is only for frequency domain (continual and scattered pilots) but not for time domain. Hence, pre-FFT non-data-aided acquisition and post-FFT data-aided acquisition and tracking algorithms are suitable. This leads to the overall CFO synchronization and compensation scheme as shown in Fig. 2.4.

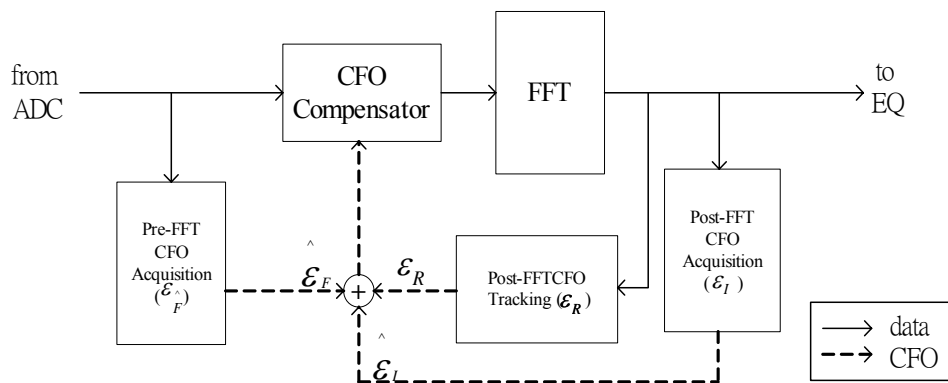


Fig. 2.4 Overall CFO synchronization and compensation scheme

The control loops of the three-stage synchronization subsystem operate in a

per-OFDM-symbol basis. When the CFO acquisition or tracking stage has generated an estimation of CFO value, the CFO compensator will calculate the effective compensation value before the beginning of the next pre-FFT OFDM symbol, and then start to compensate the updated CFO value when the next pre-FFT OFDM symbol comes.

2.3 Fractional Carrier Frequency Offset Synchronization

The estimation of fractional CFO was first proposed by Moose in 1994 [9]. This approach utilizes maximum likelihood estimation (MLE) of differential phase between two repeated training symbols in frequency domain to estimate the fractional CFO value. The estimation range is limited within ± 0.5 subcarrier space, and can be expressed as

$$\hat{\mathcal{E}}_F = \frac{1}{2\pi} \tan^{-1} \left[\frac{\text{Im} \sum_{k=-K/2}^{K/2-1} R_{1,k}^* \cdot R_{2,k}}{\text{Re} \sum_{k=-K/2}^{K/2-1} R_{1,k}^* \cdot R_{2,k}} \right] \quad (2-7)$$

where $R_{1,k}^*$ and $R_{2,k}$ are the pre-defined training symbols in frequency domain.

In WLAN IEEE 802.11a system, similar idea is exploited but different training patterns are utilized [10]. The estimation of CFO is accomplished by the aid of pre-defined short preamble and long preamble in time domain and achieves wider estimation range than Moose's approach. However, there is no any pre-defined training sequence except the continual and scattered pilots in DVB-T/H system. The former two data-aided algorithms are both not suitable solutions for our application.

From section 2.1.2, we can know that the phase of the received signal in time domain is rotated by CFO linearly according to the sample time instant t_n as (2-4) shows. When the difference of sample time instant between two received signals is equal to FFT length N , the phase error difference caused by CFO between them can be expressed as

$$\theta_l(n+N) - \theta_l(n) = 2\pi\Delta f t_{n+N} - 2\pi\Delta f t_n$$

$$\begin{aligned}
&= 2\pi\varepsilon(IN_s + N_g + n + N)/N - 2\pi\varepsilon(IN_s + N_g + n)/N \\
&= 2\pi\varepsilon = 2\pi(\varepsilon_I + \varepsilon_F). \tag{2-8}
\end{aligned}$$

Since the phase rotation of multiples of 2π can be ignored, the phase error between $r_l(n)$ and $r_l(n+N)$ is just equal to $2\pi\varepsilon_F$ and in proportion to the fractional CFO value. This phase error feature will be utilized in our proposed fractional CFO synchronization. In the proposed DVB-T/H system platform, however, no any useful training symbol can be used in time domain. So if we want to exploit the phase error feature between $r_l(n)$ and $r_l(n+N)$, the guard interval based algorithm is the most suitable solution.

In order to prevent the influence of multipath channel spread and inter-symbol interference (ISI), a cyclical prefix is inserted in front of each symbol. The cyclical prefix must be composed of partial signal in the back of the symbol, and its length has to be longer or equal to the multipath delay spread as shown in Fig. 2.5.

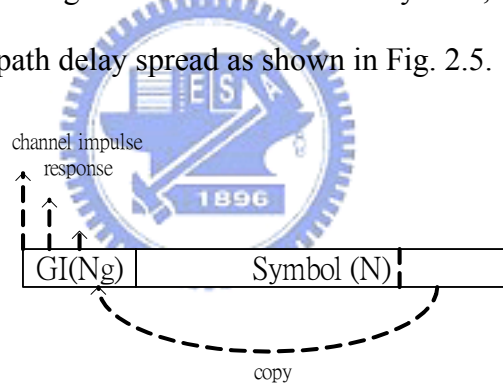


Fig. 2.5 Guard interval insertion and multipath channel spread

Because all the samples in guard interval are copied from the rear part of the symbol, the received sample $r_l(n)$ in guard interval and $r_l(n+N)$ in the symbol's tail are exactly identical when there is no any distortion exists such as multipath delay spread or CFO. As previous sections mentioned, the difference of rotated phase error between $r_l(n)$ and $r_l(n+N)$ is in proportion to the fractional CFO value ε_F . We can conclude that the tail received sample and its cyclical prefix show the same property except for a phase rotation error which is exactly $2\pi\varepsilon_F$. The estimation of fractional CFO value can be accomplished with the MLE of differential phase between guard interval and the tail of symbol [11], and can

be expressed as

$$\begin{aligned}
x &= \sum_{n=N_s-N_g}^{N_s-1} r_{l,n-N}^* \cdot r_{l,n} = \sum_{n=N_s-N_g}^{N_s-1} (r_{l,n-N}^* \cdot r_{l,n-N}) e^{j2\pi\epsilon_F} \\
&= e^{j2\pi\epsilon_F} \sum_{n=N_s-N_g}^{N_s-1} |r_{l,n-N}|^2 \\
\hat{\epsilon}_F &= \frac{1}{2\pi} \arg(x) = \frac{1}{2\pi} \tan^{-1} \left[\frac{\text{Im} \sum_{n=N_s-N_g}^{N_s-1} r_{l,n-N}^* \cdot r_{l,n}}{\text{Re} \sum_{n=N_s-N_g}^{N_s-1} r_{l,n-N}^* \cdot r_{l,n}} \right] \quad (2-9)
\end{aligned}$$

(2-9) shows that the distinguishable phase error of $\arg(x)$ is within $\pm\pi$, so the estimation range of the fractional CFO synchronization is also limited within ± 0.5 subcarrier space. In the proposed CFO synchronization scheme, the rough estimation of fractional CFO is calculated with the first symbol after symbol boundary is decided. And then the estimated fractional CFO value $\hat{\epsilon}_F$ will be sent to the CFO compensator before data being sent to FFT demodulator as Fig. 2.4 shows.

If AWGN is the only external distortion, the accuracy of the fractional CFO synchronization will be very excellent because the correlation of guard interval and tail of symbol can average the noise induced by AWGN. However, the DVB-T/H system is an outdoor wireless communication application and robust ability to long delay spread of multipath channel is necessary. As Fig. 2.5 shows, the delay spread of multipath channel will affect the data of the front portion of the guard interval directly especially when the length of guard interval is relatively short (2k mode, $N_g / N = 1/32$). In order to reduce the effect of multipath delay spread, several beginning samples of the guard interval must be discarded, and (2-9) can be rewritten as

$$\hat{\varepsilon}_F = \frac{1}{2\pi} \arg(x) = \frac{1}{2\pi} \tan^{-1} \left[\frac{\text{Im} \sum_{n=N_s-N_g+y}^{N_s-1} r_{l,n-N}^* \cdot r_{l,n}}{\text{Re} \sum_{n=N_s-N_g+y}^{N_s-1} r_{l,n-N}^* \cdot r_{l,n}} \right] \quad (2-10)$$

where y is the number of discarded samples. However, discarding too many samples will also degrade the averaging performance. The optimal value of y will be shown by simulation result in chapter 3.

2.4 Integral Carrier Frequency Offset Synchronization

From previous section, we can know that the time domain guard interval correlation algorithm can only deal with the rotated phase error caused by the fractional CFO value. The imperfect effect caused by the integral CFO should be monitored and synchronized in frequency domain. Thanks to the compensation of $\hat{\varepsilon}_F$, the residual fractional CFO ε_R is relatively smaller ($\varepsilon_R \leq 0.02$) and the ICI noise is also neglected. In essence, the k -th transmitted subcarrier shows up at FFT output bin with subcarrier index $k + \varepsilon_I$ as Fig. 2-3 (b) shows. The subcarrier index shift, which is just equal to the integral CFO ε_I , must now be detected by using the pre-defined training sequence (continual and scattered pilots) or the null subcarriers. In later sections, some different algorithms of integral CFO synchronization will be illustrated and discussed.

2.4.1 Conventional Pilots Based Approach

The DVB-T/H standard defines continual and scattered pilots for synchronization and equalization in frequency domain [3]. The signal power of the two kinds of pilots is at boosted power level and larger than the data and null subcarriers. The only difference between continual and scatter piloted is their subcarrier index. The continual pilots locate at fixed subcarrier index and do not shift as OFDM symbol number increases. However, scattered

pilots are inserted every 12 subcarriers and have an interval of 3 subcarriers in the next adjacent symbol. In general, the continual pilots based integral CFO synchronization algorithms are the most widely used because of its good performance in low SNR and mobile environment [12][13]. The main idea of this approach is based on the MLE theory. In the first step, the correlation between two continual pilots at the same subcarrier index for two successive symbols in the frequency domain based on shifting the pilot positions is calculated, and can be expressed as

$$C_i = \left| \sum_{k=P_i} R_{l-1,k}^* \cdot R_{l,k} \right|, |i| \leq m \quad (2-11)$$

where C_i is the correlation value at the i -th shift location, $P_i = [p_1 + m, p_2 + m, \dots, p_p + m,]$ are the positions of the subcarriers to be correlated in two successive symbols, and m is the estimation range. The integer CFO value ε_l is then estimated by detecting the offset position i where the value C_i is maximized as

$$\hat{\varepsilon}_l = \underset{i}{\text{max}} (C_i) \quad (2-12)$$

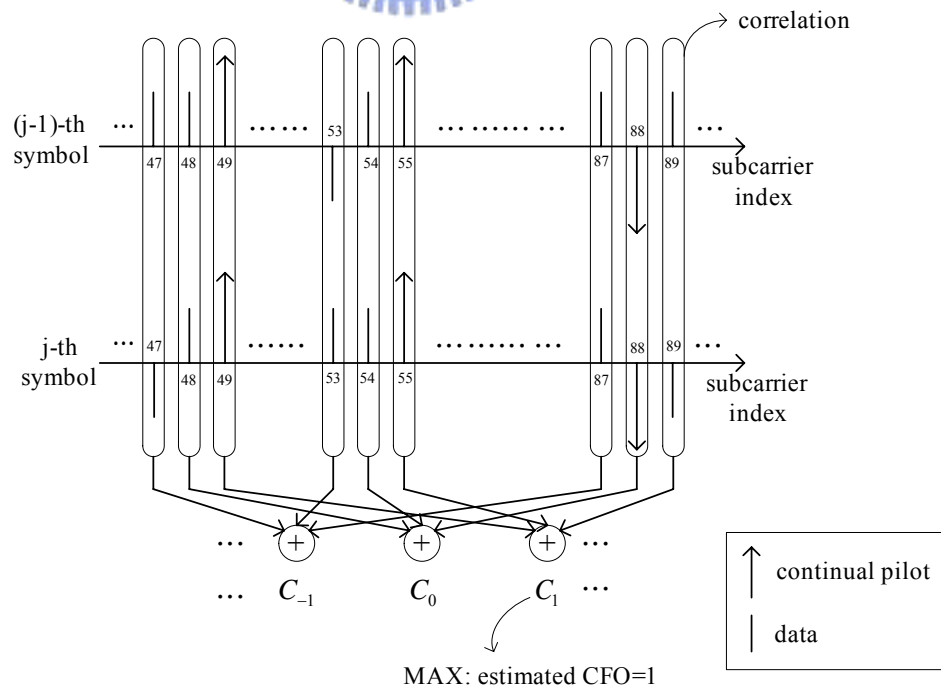


Fig. 2.6 Received signal in frequency domain when CFO=1 subcarrier space

Fig. 2.6 shows the received signal according to the subcarrier in frequency domain when the integral CFO is equal to 1 subcarrier space. In DVB-T/H 2k mode, the positions of continual pilots should be 0, 48, 54, 87.... Accordingly, if the maximum value of C_i is obtained from subcarriers 1, 49, 55, 88..., the estimated integral CFO is 1 because the position of maximum correlation is achieved one subcarrier position away from the original continual pilots. Because the continual pilots are transmitted at boosted power level, the power difference of correlation values is still apparent and not affected by strong noise even in low SNR and deep delay spread channel condition. The total number of multiplication when the acquisition of integral CFO is finished can be expressed as

$$M = (2m + 1) \cdot (P \cdot 4 + 2) \quad (2-13)$$

where M is the total number of multiplication, and P is the number of correlated pilots, respectively. In DVB-T/H system, P is 45, 89, and 177 for 2k, 4k, and 8k mode. Apply (2-13) we can see that as the search range increases, if all of the continual pilots are used for estimation, the total number of multiplication will increase enormously. For example, if the desired search range m is 60 for 2k mode when using all continual pilots, the number of multiplication will raise up to 22022. For low power consideration, such large number of multiplication should be avoided. The tradeoff between estimator performance and power consumption has become an important task for the integral CFO acquisition.

Besides the continual pilots based approach, another algorithm based on both continual and scattered pilots (CP+SP) was also proposed [14]. This algorithm calculates the correlation between possible 4 types of CP+SP patterns with the shifted received symbol in frequency domain. By detecting the peak value of the correlation result among the 4 CP+SP patterns, the integral CFO and the scattered pilot mode can be estimated at the same time, and can be expressed as

$$\hat{\mathcal{E}}_I = \max_i \left| \sum_{k=1}^{P'} R_{l,z,k+i} \cdot Y_{z,k}^* \right|, z \in [0, 1, 2, 3] \quad (2-14)$$

where P' is the total number of CP+SP, $Y_{z,k}$ is the z type CP+SP sequence, and z is the subcarrier index pattern of 4 possible types of CP+SP, respectively. Although this approach can acquire the scattered pilot mode and the integral CFO at the same time, the computational complexity also rises to about 4 times of the continual pilots based one and leads to more power consumption.

2.4.2 Conventional Guard Band Based Approach

In DVB-T/H system, the number of subcarriers K within an OFDM symbol is chosen smaller than the symbol length N to provide that so-called “guard bands” at the edges of the transmission spectrum are left free. Hence all the subcarriers within guard-bands are composed of null subcarriers and the transmitted signal power is zero. According to the DVB-T standard, the signal power of the useful data subcarrier is normalized to 1, and the power of the reference pilots is 16/9 [3]. By exploiting the feature of power difference, a guard band power detection based algorithm for integral CFO acquisition was proposed by Kim in 1997 [15]. This algorithm utilizes the guard bands in both sides of spectrum as a moving window to search the subcarrier index shift value caused by the integral CFO. The main idea is that when the useful signal component (data or pilot subcarriers) is not within the moving window, the total component power within the moving window includes only noise component. So when the power of the moving window reaches minimum, the shift value of the window is equal to the shift value of signal spectrum due to the integral CFO, and can be expressed as

$$\hat{\mathcal{E}}_I = \min_i \left\{ \sum_{k=K_{\min}-w}^{K_{\min}-1} |R_{l,k+i}|^2 + \sum_{k=K_{\max}+w}^{K_{\max}+1} |R_{l,k+i}|^2 \right\}, |i| \leq m \quad (2-15)$$

where w is the width of the moving window at both sides of the guard band and is set as 5.

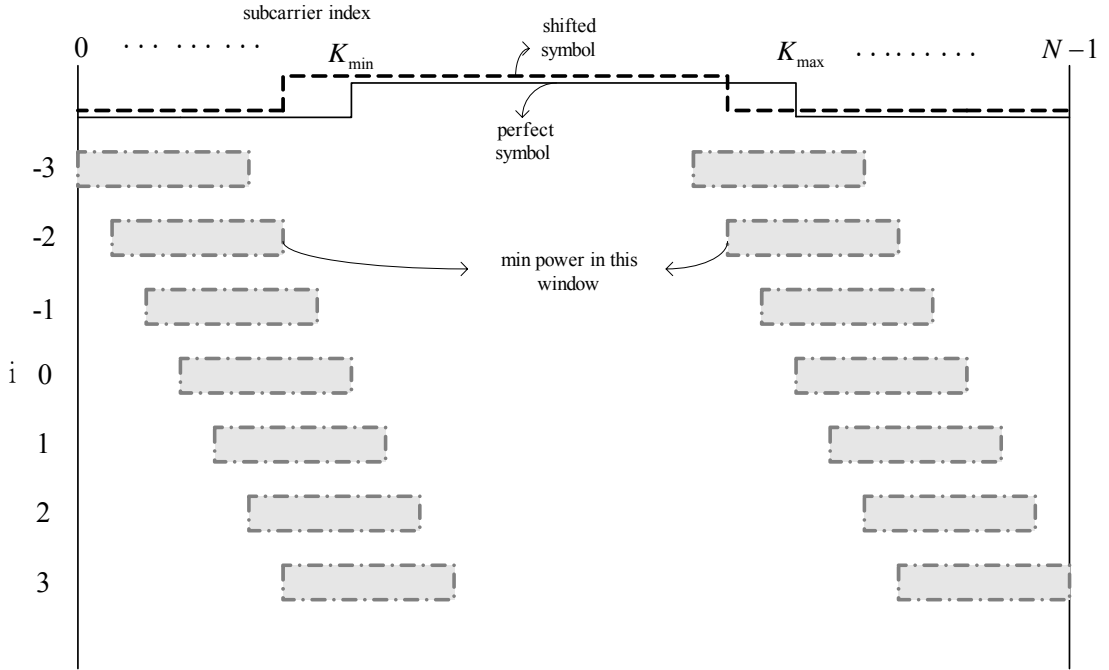


Fig. 2.7 Received symbol in frequency domain when CFO is -2

Fig. 2.7 shows the received symbol spectrum in frequency domain according to subcarrier index when the integral CFO is -2 subcarrier space. As we can see the minimum power appears in the moving window where i is -2 because it does not include any data or pilot component. The total number of multiplication M required for the acquisition of integral CFO can be expressed as

$$M = (w + 2m) \cdot 4 \quad (2-16)$$

From (2-16), we can find that the number of multiplication M could be reduced effectively by using small moving window width w . However, small w may lead this algorithm to worse performance in low SNR and deep frequency selective fading environment. So the trade-off between w and M should be treated very carefully.

In order to improve the performance of the conventional guard band power detection based algorithm, another modified guard band power detection method was proposed [16]. This algorithm modifies the structure of the symbol spectrum and inserts additional null subcarriers within the useful subcarriers to reduce the influence from ICI noise and deep frequency selective fading. However, the modification conflicts with the DVB-T/H standard

and can not be applied for our system platform.

2.4.3 Proposed 2-stage Approach

From previous sections, we can conclude that neither the continual pilots based algorithm nor the guard band power detection based algorithm can satisfy good performance and low computational complexity at the same time. Besides, the number of multiplication of all these algorithms is in proportion to the search range. If we want to let the integral CFO estimator work in low SNR and deep frequency selective fading environment and search large range CFO with low computational complexity, none of these algorithms is the best choice. In order to solve this problem, a 2-stage integral CFO acquisition algorithm is proposed as Fig 2.8 shows. The objective of the first stage is to recognize whether the integral CFO value ε_f is positive or negative (i.e. to find whether the direction of subcarrier shift due to integral CFO is right or left) with a low complexity guard band based algorithm. Once the first stage finishes and finds the direction of the subcarrier shift, the search range and the number of multiplication can be reduced half at the same time. In the second stage, the accurate integral CFO value ε_f will be acquired along the direction estimated by the first stage with the proposed continual pilots based algorithm or guard band based algorithm. The detailed content of the proposed 2-stage approach will be illustrated in later sections.

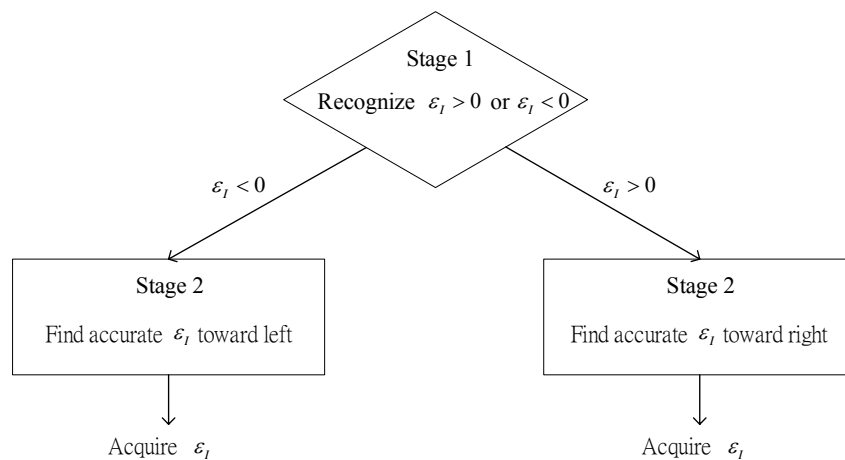


Fig. 2.8 Proposed 2-stage integral CFO algorithm scheme

2.4.4 The First Stage of the Proposed Approach

The main task of this stage is to find whether the integral CFO value ε_l is positive or negative fast and efficiently, so a left window and a right window that composed of w_1 guard band null subcarriers and w_1 data subcarriers at the boundary between guard band and data are exploited. In the first step, the summation of signal power of two successive OFDM symbols based on the position of left and right window is calculated separately. Once the integral CFO value ε_l is not equal to zero, the subcarrier distribution of guard band and data within the left and right window will be imbalanced. So in the second step, we compare the calculated correlation power to decide whether the integral CFO value ε_l is positive or negative, and can be expressed as

$$\begin{aligned}
 L &= \sum_{k=left} \left[|R_{l-1,k}|^2 + |R_{l,k}|^2 \right] \\
 R &= \sum_{k=right} \left[|R_{l-1,k}|^2 + |R_{l,k}|^2 \right] \\
 L > R, \varepsilon_l \leq 0 \quad \text{or} \quad L < R, \varepsilon_l \geq 0
 \end{aligned} \tag{2-17}$$

where $left = [K_{min} - w_1, K_{min} - w_1 + 1, \dots, K_{min} - 1, K_{min}, K_{min} + 1, \dots, K_{min} + w_1 - 1]$, $right = [K_{max} - w_1 + 1, K_{max} - w_1, \dots, K_{max} - 1, K_{max}, K_{max} + 1, \dots, K_{max} + w_1]$, and w_1 is the window width, respectively.

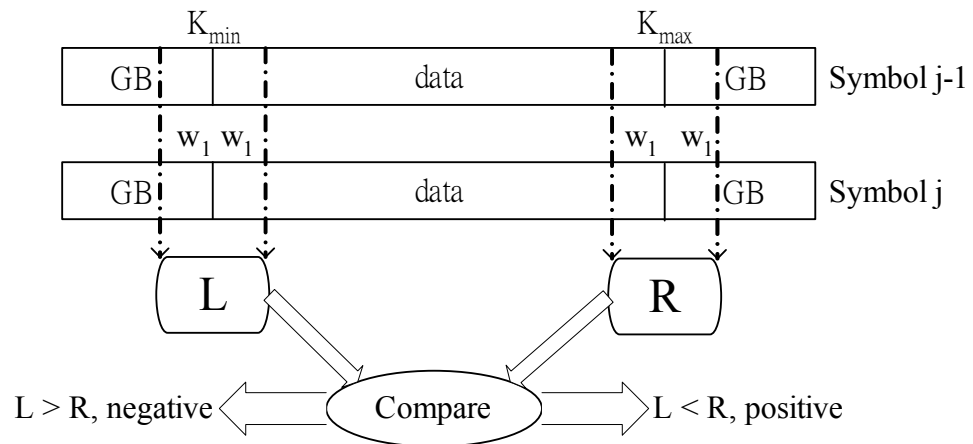


Fig. 2.9 The first stage of the proposed integral CFO estimator

As shown in Fig. 2.9, we can see that if the integral CFO value ε_I is larger than zero, the received subcarrier will shift toward right and the number of guard band signal will be more than that of the data signal in the left window. Also in the right window, the number of the guard band signal will be less than that of the data signal. The power difference between the left and right window will appear and help us to decide whether the integral CFO value ε_I is positive or negative. The total number of multiplication of the first stage can be expressed as

$$M = 8 \cdot w_1 \quad (2-18)$$

From (2-18) we can know that the number of multiplication of the first stage is not affected by the estimation range m and low complexity calculation can be achieved by choosing smaller window width. However, too small window width will affect the performance of the first stage. The optimal window width will be shown by simulation result in chapter 3.



2.4.5 The Second Stage of the Proposed Approach

By the aid of the first stage, the search range of the second stage can be reduced from $\pm m$ to m . However, the result of the first stage may be incorrect while the integral CFO value ε_I is smaller than the window width w_1 in deep frequency selective fading channel environment. In order to prevent estimation error, the search range should be extended from m to $m + w_1$, implying that we should add more w_1 points to the search range toward the reverse direction to assure correct acquisition result when the integral CFO value ε_I is near zero in deep frequency selective fading channel.

Once the search range of the second stage is decided, there are still various algorithms can be applied for acquisition the accurate integral CFO value ε_I . The trade-off between estimator performance and computational complexity, however, still exists among the previous mentioned algorithms. Considering acceptable acquisition performance and efficient

computation load, a reduced continual pilot based algorithm and a guard band power detection based algorithm are proposed for the acquisition in the second stage, and will be illustrated in later sections.

(1) Proposed Reduced Continual Pilot Based Approach

From (2-13), we can find that the number of multiplication of the conventional continual pilot based approach is in proportion to not only the search range m but also the number of utilized continual pilot P . In order to achieve efficient computational load, the number of utilized continual pilot should be reduced with the search range at the same time. Hence a reduced continual pilot based approach is proposed. The main feature of the proposed reduced continual pilot based algorithm for the second stage integral CFO acquisition is similar to the conventional continual pilot based one. But the proposed one exploits only a part of the continual pilot instead of all of them to reduced the number of multiplication, and can be expressed as

$$\hat{\mathcal{E}}_l = \max_i \left| \sum_{k=P_{r,i}} R_{l-1,k}^* \cdot R_{l,k} \right| \quad (2-19)$$

where $P_{r,i}$ is the shifted subcarrier index of the selected continual pilots, $-m \leq i \leq w_1$ while negative value estimated by the first stage, and $-w_1 \leq i \leq m$ while positive value, respectively. The number of multiplication for the proposed reduced continual pilot approach can be expressed as

$$M = (m + w_1 + 1) \cdot (P_r \cdot 4 + 2) \quad (2-20)$$

where P_r is the total number of the correlated continual pilots. Because the power difference between pilot and data subcarrier is very significant, it is not necessary to use all of the continual pilots and the acquisition performance is still acceptable to meet lower computational load. As (2-20) shows, the number of multiplication can be reduced effectively.

The optimal value of the number of the selected continual pilots will be chosen by simulation and shown in chapter 3.

(2) Proposed Guard Band Power Detection Based Approach

As previous sections mentioned, the conventional guard band power detection based algorithm requires fewer number of multiplication and performs worse performance in low SNR and deep frequency selectively fading environment because it utilizes only one OFDM symbol. In order to utilize the advantage of lower computational complexity and to improve the performance in critical channel condition, we propose a new guard band power detection based algorithm. By the aid of the proposed first stage, the search range of the second stage can be reduced effectively and more OFDM symbols can be utilized to improve the acquisition performance. Thus the proposed guard band power detection based algorithm still keeps the moving window scheme and calculates the summation of signal power within three successive OFDM symbols, and can be expressed as

$$\hat{\mathcal{E}}_l = \min_i \left\{ \sum_{k=K_{\min}-w_2}^{K_{\min}-1} \left[|R_{l,k+i}|^2 + |R_{l-1,k+i}|^2 + |R_{l-2,k+i}|^2 \right] + \sum_{k=K_{\max}+w_2}^{K_{\max}+1} \left[|R_{l,k+i}|^2 + |R_{l-1,k+i}|^2 + |R_{l-2,k+i}|^2 \right] \right\} \quad (2-21)$$

where w_2 is the width of the moving window at both sides of the guard band, $-m \leq i \leq w_1$ while negative value estimated by the first stage, and $-w_1 \leq i \leq m$ while positive value, respectively. As Fig. 2.10 shows, by the use of summation within three successive OFDM symbols, the distortion induced by noise in severe environment can be decreased effectively.

The number of multiplication can be expressed as

$$M = (w_2 + m + w_1) \cdot 12 \quad (2-22)$$

Compared (2-22) with (2-16), we can see that the total number of multiplication of the proposed guard band power detection based approach consumes about 1.5 times of that of the conventional approach. However, the acquisition performance is improved significantly. The

detailed performance simulation and comparison will be illustrated in chapter 3.

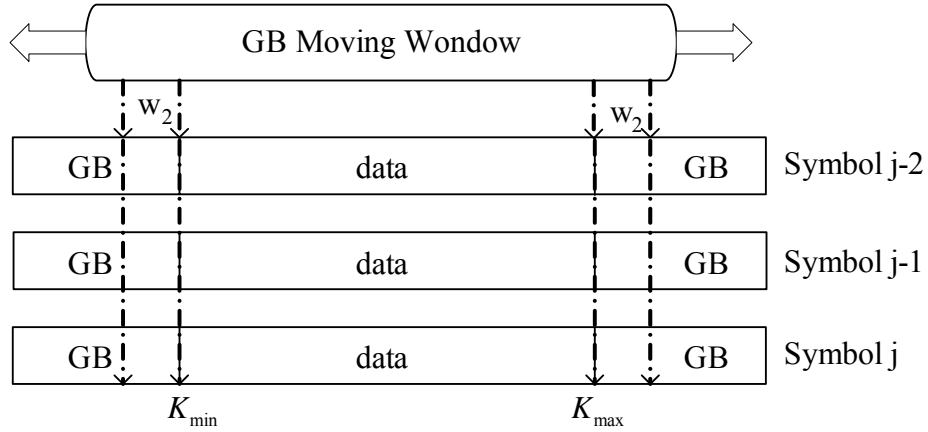


Fig. 2.10 The proposed guard band power detection based approach

2.5 Residual Carrier Frequency Offset Synchronization

After the acquisition stage estimates the integral and most of the fractional CFO value, the residual CFO value is usually less than 1 to 2 percent of the subcarrier space. However, the phase error induced by such small value of CFO in time domain still affects the system performance for long time receiving operation. As Fig. 2.2 shows, the accumulative phase error when residual CFO value is 0.01 still exceeds π while the received number of data is more than 10,000. Besides, the Doppler effect in mobile environment also introduces small drift to CFO. Therefore the tracking of residual CFO is necessary and has to operate continuously until the reception is turned off.

Generally speaking, the residual CFO value ε_R is usually very small. Thus only fractional CFO estimation is sufficient. In particular, the estimation of the residual CFO at tracking stage requires precise and low variation result. Therefore in our DVB-T/H system platform, the tracking stage of CFO is divided into two parts. The first part estimates the residual CFO value symbol by symbol followed by a PI (proportional-integral) loop filter to reduce the variation. The tracking loop of the CFO synchronization is shown in Fig. 2.11.

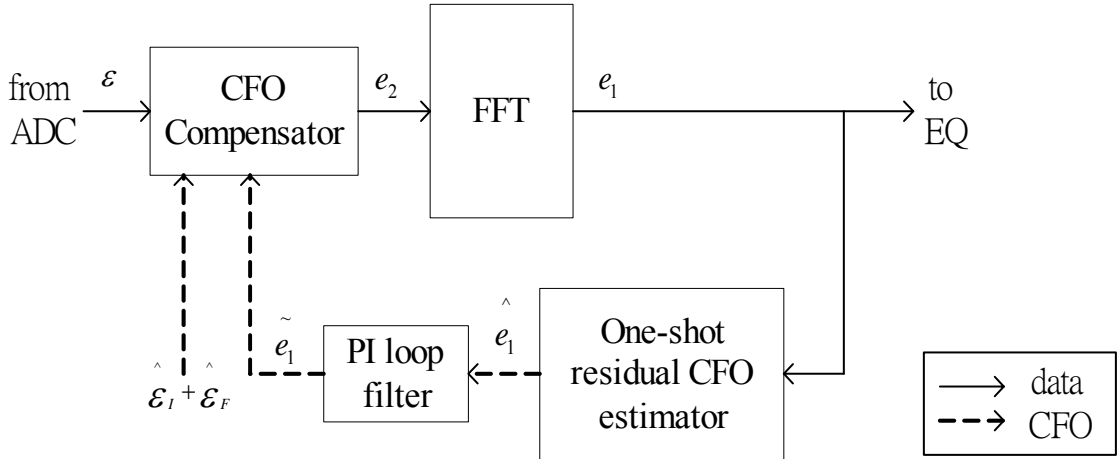


Fig. 2.11 The tracking loop of the CFO synchronization

As shown in Fig. 2.11, e_1 is the residual CFO value of the first iteration of the tracking loop. After the estimation of e_1 , the output of the residual CFO estimator \hat{e}_1 will be post-processed by the PI loop filter. When the second iteration starts, the CFO compensator will compensate the incoming data with the updated CFO value $\hat{\mathcal{E}}_I + \hat{\mathcal{E}}_F + \tilde{e}_1$ and then get the next residual CFO error e_2 of the second iteration. As the CFO tracking loop works iteratively, the residual CFO error will be minimized.

2.5.1 Residual CFO Estimation

The objective of the residual CFO estimator is to estimate the residual CFO error value precisely and fast. As previous section mentioned, only fractional CFO synchronization is sufficient for this estimator. Considering hardware integration and resource reuse, the fractional CFO estimator described in section 2.3 may can be utilized for the residual CFO estimator. However, the non-data-aided algorithm that exploits the guard interval is very sensitive to the inter-symbol interference introduced by the multipath delay spread and the estimated result may be not precise enough for the residual CFO estimation in deep delay fading environment. Only roughly fractional CFO value can be obtained with this approach. Therefore an efficient data-aided algorithm that employs the pre-defined continual pilots is

applied for the residual CFO estimator.

After most of the CFO value is estimated and compensated, the residual CFO value is usually less than 1 to 2 percent of the subcarrier space and the ICI noise is small enough to be neglected. As (2-3) shows, regardless of the ICI term, the phase error caused by the residual CFO error and SCO at the k -th subcarrier of the l -th OFDM symbol in frequency domain can be expressed as

$$\varphi_l(k) = 2\pi\varepsilon_R(lN_s + N_g)(1 + \zeta) / N + \frac{2\pi k}{N}(lN_s + N_g)\zeta + \phi_l(k) \quad (2-23)$$

where $\phi_l(k)$ is the phase of the channel frequency response $H_{l,k}$. If the channel is a slowly fading channel ($\phi_l(k) \approx \phi_{l-1}(k)$), the difference of phase rotation between two successive OFDM symbols is represented as

$$\begin{aligned} \varphi'_l(k) &= \varphi_l(k) - \varphi_{l-1}(k) \\ &= \frac{2\pi\varepsilon_R N_s}{N} + \frac{2\pi\varepsilon_R N_s \zeta}{N} + \frac{2\pi k N_s \zeta}{N} \\ &\approx \frac{2\pi\varepsilon_R N_s}{N} + \frac{2\pi k N_s \zeta}{N} \end{aligned} \quad (2-24)$$

The second term $\frac{2\pi\varepsilon_R N_s \zeta}{N}$ can be ignored since the product of $\varepsilon_R \cdot \zeta$ is usually less than 2.0×10^{-6} . From (2-24) we can know that the residual CFO ε_R causes mean phase error and the SCO ζ causes linear phase offset between two consecutive OFDM symbols. If we take two adjacent continual pilots of arbitrary two consecutively received OFDM symbols, the phase rotation is shown in Fig. 2.12 [17]. The total phase rotation includes the effects of symbol timing offset, residual CFO and SCO. As we can see from Fig. 2.12, the magnitude of phase rotation induced by symbol timing offset is identical and in proportion to the subcarrier index among the two symbols. However, in the current symbol, the effect of residual CFO and SCO are accumulated in the phase of the previous symbol, where the residual CFO induces mean phase and SCO generates linear phase. Thus, we must estimate the residual CFO as well as the SCO by computing the phase rotation between two successive symbols.

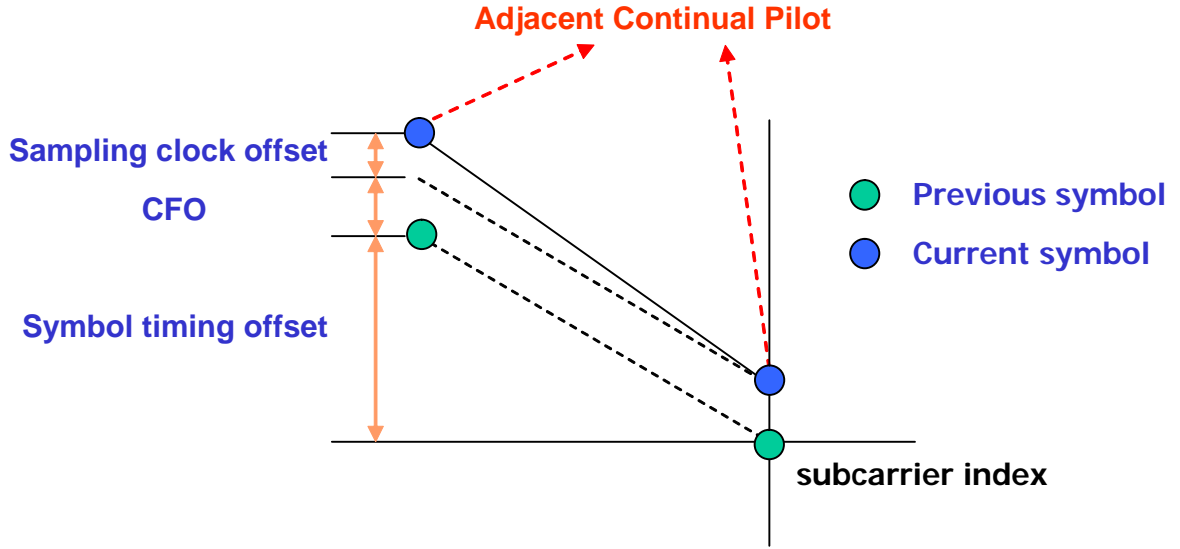


Fig. 2.12 Phase rotation between two successive OFDM symbols

Since the phase error caused by residual CFO is identical within one OFDM symbol, the continual pilots which have fixed subcarrier index are exploited to estimate the residual CFO. In general, the residual CFO and the SCO are estimated jointly because their effects of phase rotation are uncorrelated. Thus a joint residual CFO and SCO estimation algorithm is applied as

$$\begin{aligned}
 \hat{\mathcal{E}}_R &= \frac{1}{2\pi(1 + N_g / N)} \cdot \frac{1}{2} \cdot (\varphi_{2,l} + \varphi_{1,l}) \\
 \hat{\zeta} &= \frac{1}{2\pi(1 + N_g / N)} \cdot \frac{1}{K/2} \cdot (\varphi_{2,l} + \varphi_{1,l}) \\
 \varphi_{1|2,l} &= \arg\left[\sum_{k \in C_{1|2}} R_{l,k} \cdot R_{l-1,k}^* \right]
 \end{aligned} \tag{2-25}$$

where C_1 denotes the subcarrier index set of continual pilots which locates in the left half ($k \in [0, (K-1)/2)$), and C_2 denotes the subcarrier index set of continual pilots which locates in the right half ($k \in ((K-1)/2, K_{\max}]$) of the OFDM symbol spectrum, respectively. Applying correlation of continual pilots within two successive OFDM symbols and accumulating the correlation results in two parts lead to the so-called CFD/SFD (carrier frequency detector / sampling frequency detector) algorithm [18]. The summation of $\varphi_{2,l}$ and $\varphi_{1,l}$ can compute mean phase error while subtraction of $\varphi_{2,l}$ and $\varphi_{1,l}$ produces the

linear phase error. As a result, the residual CFO and SCO can be estimated jointly by multiplying different coefficients.

Besides the continual pilots based approach, some other scattered pilots based approaches are also presented in [14] and [19]. [14] proposes a residual CFO estimator that exploits the continual and scattered pilots between the l -th and the $(l-4)$ -th OFDM symbol. The equation of this approach is very similar to (2-25) except the correlated symbols and pilots. The main feature of this algorithm is to use more pilots to reduce the distortion caused by AWGN and ICI noise. However, the convergence speed is extended about 2.5 times longer than that of the CFD/SFD algorithm because it utilizes the l -th and the $(l-4)$ -th OFDM symbol. In [19], the residual CFO estimator exploits the scattered pilots within two successive OFDM symbols and has similar equation with (2-25). However, the subcarrier index of scattered pilots of two successive OFDM symbols is not identical and has a difference of 3. The estimated phase error between two scattered pilots is also distorted by the symbol timing offset. However, the symbol timing offset is an unknown factor and can not be estimated precisely by symbol synchronizer. So the estimation result of this approach is not reliable only if precise symbol offset value is estimated.

2.5.2 Residual CFO Tracking Loop Filter

In order to reduce the variation of the estimated residual CFO, a PI loop filter is utilized in our CFO synchronization design [20]. The PI loop filter is composed of two paths. The proportional path multiplies the estimated residual CFO by a proportional factor K_p . The integral path multiplies the estimated residual CFO by an integral factor K_i and then integrates the scaled value by using an adder and a delay element. The block diagram of the PI loop filter is shown as Fig. 2.13.

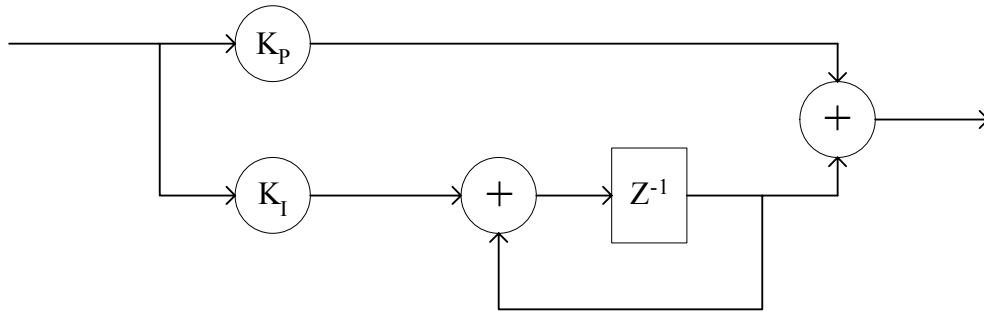


Fig. 2.13 Block diagram of PI loop filter

The transform function of the PI loop filter can be represented as

$$H(z) = K_p + K_i \frac{Z^{-1}}{1 - Z^{-1}} \quad (2-26)$$

For small loop delay and $K_i \ll K_p \ll 1$, the standard deviation of the steady-state tracking error is expressed as

$$\sigma(e') = \sqrt{K_p/2} \cdot \sigma(e) \quad (2-27)$$

where e is the estimation error of the residual CFO estimator and e' is the steady-state tracking error. The close-loop tracking time constant is approximately given by

$$T_{loop} \approx 1/K_p \quad (2-28)$$

So from (2-27) and (2-28) we can find that there is a tradeoff between steady-state tracking error and tracking convergence speed. In our proposed DVB-T/H platform, the loop parameter K_p is chosen as a larger value to increase the convergence speed in the beginning of tracking, and then switched to a smaller value to reduce the steady-state tracking error variation.

Chapter 3 .

Simulation and Performance Analysis

In this chapter, the overall simulation platform built for DVB-T/H system will be illustrated first. The channel model and some other distortion source such as Doppler delay spread and SCO model will be discussed later. Finally, the performance analysis of the proposed CFO synchronization scheme and comparison with state of the art will be performed.

3.1 Simulation Platform

In order to verify the performance of the proposed CFO synchronization scheme, a complete DVB-T/H baseband simulation platform is constructed in Matlab. The block diagram of the overall simulation platform is shown as Fig. 3.1.

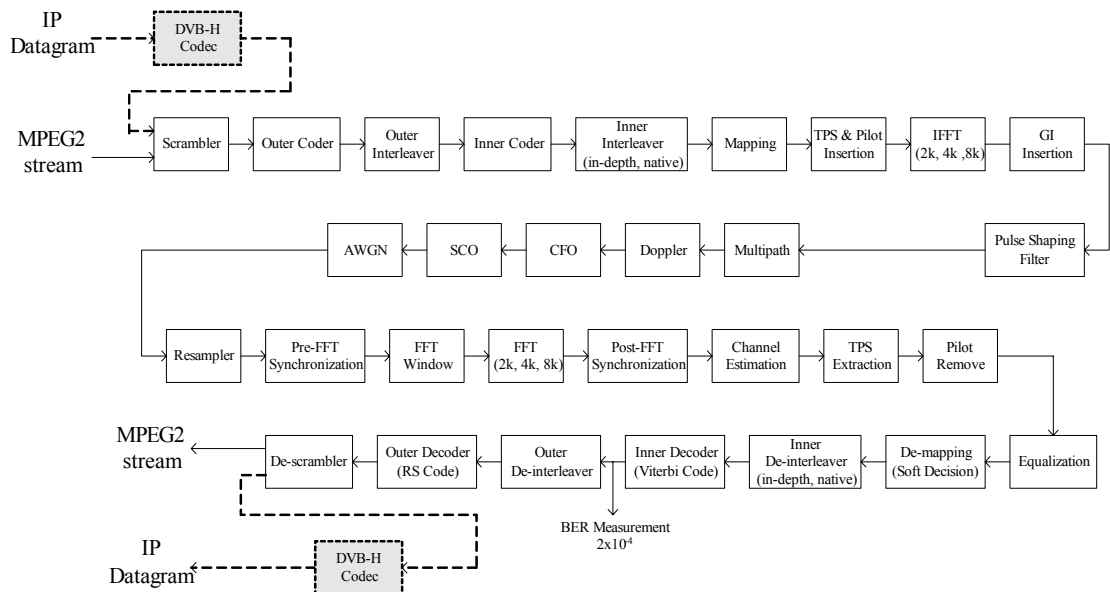


Fig. 3.1 Overall DVB-T/H platform

As shown in Fig. 3.1, the blocks with dotted line is the specific function blocks for DVB-H system. By adding support of 4k IFFT/FFT, in-depth interleaving, and additional TPS information, the developed DVB-T system platform can share most of the function blocks with DVB-H system at the same time. The platform is composed of transmitter, channel, and receiver. A typical transmitter that receives data from MPEG2 encoder or IP datagram is completely established. The transmitter consist the full function of FEC blocks and OFDM modulation blocks. The coding rate, interleaving mode, constellation mapping mode, IFFT length, and guard-interval length are all parameterized and able to be selected while simulation. An oversampling and pulse shaping filter is added before data entering channel to simulate discrete signal as far as continuously. The oversampling rate is also parameterized and can be chosen according to the simulation accuracy. The roll-off factor of the pulse-shaping filter is chosen as a normal value $\alpha = 0.15$ because it is not defined in the DVB-T/H standard.

Various distortion models are adopted in the channel model to simulate real mobile environment such as multipath fading, Doppler spread, AWGN, CFO, and SCO. In practically, there are still some imperfect effects which contain co-channel interference, adjacent-channel interference, phase noise, and common phase error caused by imperfect front-end receiving. However, the distortion of these imperfect effects is relatively smaller compared with effective time-varying channel response caused by Doppler spread, CFO, and SCO. Therefore these effects are neglected in our simulation platform.

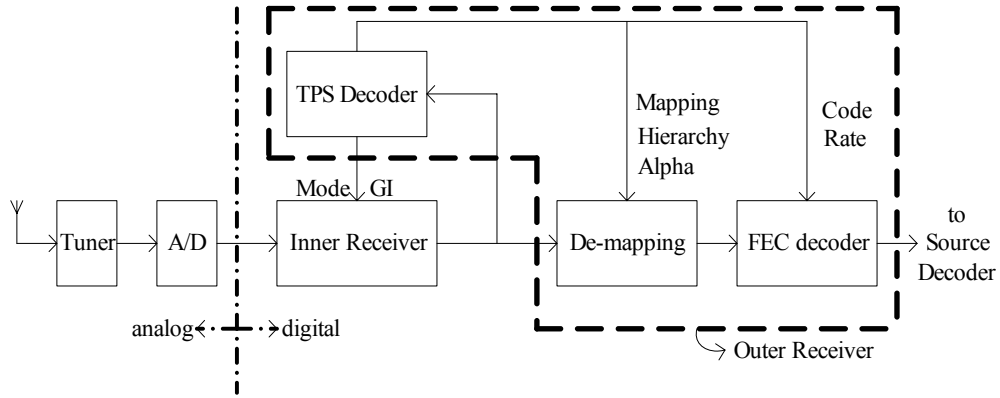


Fig. 3.2 The baseband receiver design

The baseband receiver in our system platform can be divided into inner receiver and outer receiver as Fig. 3.2 shows. The inner receiver includes all of the timing and frequency synchronization function, FFT demodulation, channel estimation, equalization, and pilot remove blocks. The outer receiver consists of other functional blocks that following the de-mapping. The transmission parameters extracted by TPS decoder such as constellation mapping mode and Viterbi code rate will be sent the relative blocks as control parameters. Besides, the extracted TPS parameter such as guard interval length and IFFT/FFT mode should be checked all the time during online receiving to prevent synchronization error. Once TPS check fail occurs, the acquisition and tracking of inner receiver must be shut down and then restart all the synchronization schemes. As for bit-error-rate (BER) measurement, the DVB-T standard defines quasi error-free condition, which means less than one uncorrelated error event per hour, while the BER of the output of the Viterbi decoder is equal to 2×10^{-4} . Therefore, in order to verify the overall system performance, the BER after Viterbi decoder should be measured.

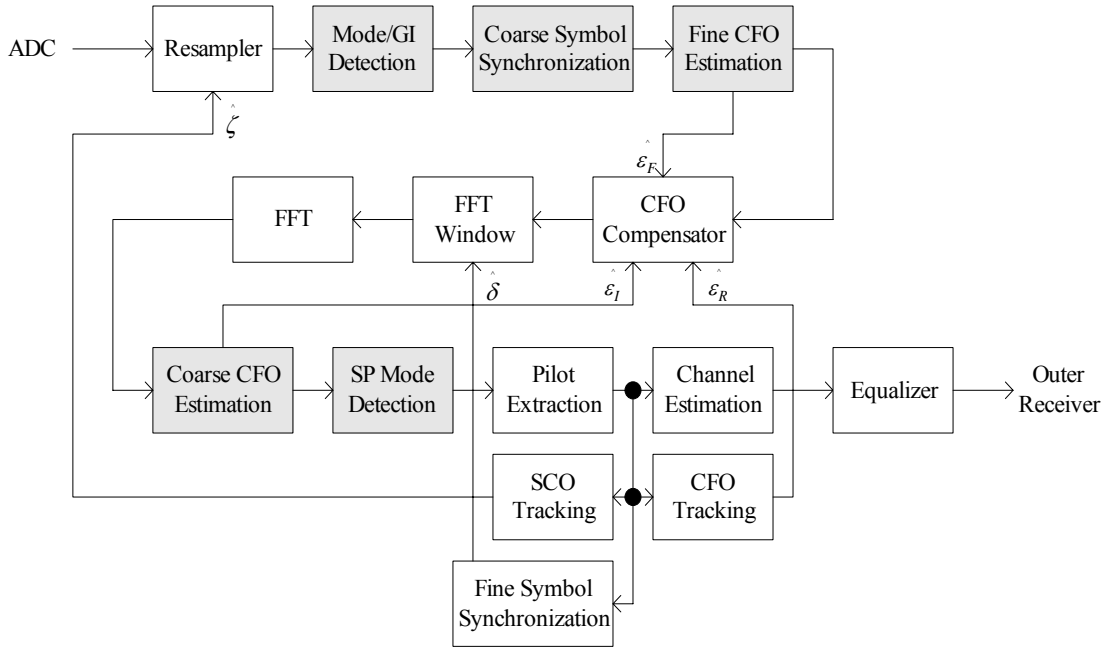


Fig. 3.3 Functional blocks of inner receiver

Fig. 3.3 shows the detail functional blocks of the inner receiver. The main functional blocks consists of symbol timing offset synchronization, carrier frequency offset synchronization, SCO synchronization, channel estimation, and equalizer, respectively. The acquisition parts (gray color) only operate in the beginning of the receiving and then are turned off when the tracking parts work, and the tracking parts works all the time until the receiver is turned off or TPS check error occurs. In this thesis, we only focus on the performance analysis of the CFO synchronization scheme. The detailed discussion of other functional blocks such as timing synchronization and channel estimation will be neglected in this work and can be found in [21].

3.2 Channel Model

The typical baseband equivalent channel model for DVB-T/H system platform is shown as in Fig. 3.4. The transmitted data will pass through multipath fading, Doppler delay spread, CFO, SCO, and AWGN in turn. The effects of co-channel interference, adjacent-channel interference, phase noise, and common phase error are neglected in our simulation. In the

following sections, the detailed effect of each channel distortion will be illustrated.

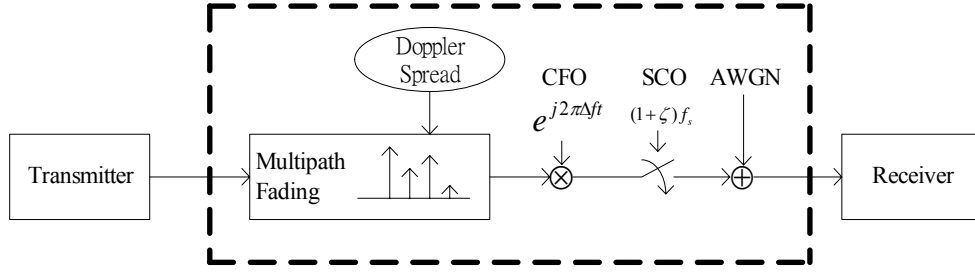


Fig. 3.4 Channel model of DVB-T/H system

3.2.1 Multipath Fading Channel Model

In wireless communication transmission, the multipath fading is caused by the reception through different paths with different time delay and power decay. In DVB-T standard, two types of multipath fading channel model are specified [3]. The fixed reception condition is modeled by Ricean channel (Ricean factor = 10dB) while the portable reception is modeled by Rayleigh channel. The full 20-tap Ricean and Rayleigh channel was used with floating point tap magnitude and phase values with tap delay accuracies rounded to within 1/2 of duration for practical discrete simulation. The channel models can be generated from the following equations where $x(t)$ and $y(t)$ are input and output signals respectively

$$\text{Rayleigh: } y(t) = \frac{\sum_{i=1}^{20} \rho_i e^{-j\theta_i} x(t - \tau_i)}{\sqrt{\sum_{i=1}^{20} \rho_i^2}} \quad (3-1)$$

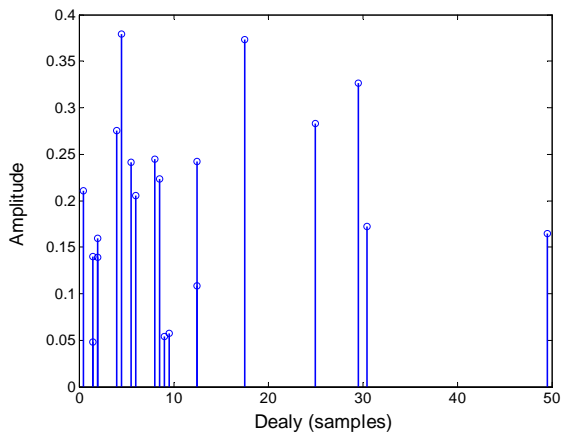
$$\text{Ricean: } y(t) = \frac{\rho_0 x(t) + \sum_{i=1}^{20} \rho_i e^{-j\theta_i} x(t - \tau_i)}{\sqrt{\sum_{i=0}^{20} \rho_i^2}} \quad (3-2)$$

where ρ_i is the attenuation of the i -th path, θ_i is the phase shift from scattering of the i -th path, and τ_i is the relatively delay of the i -th path, respectively. The detailed value of these parameters is listed in table B.1 of [3]. The rms delay of Rayleigh and Ricean channel is $1.4426 \mu s$ (about 13 samples) and $0.4491 \mu s$ (about 4 samples). From the above two

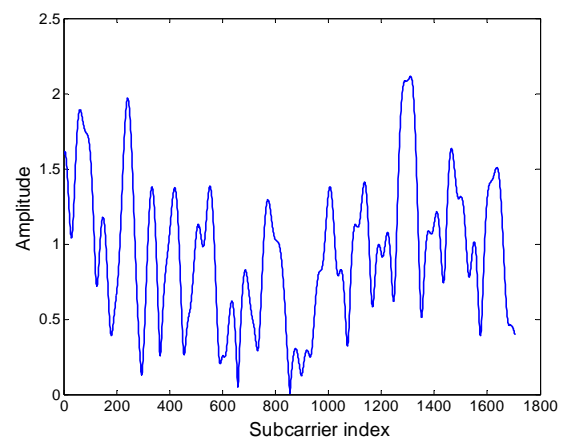
equations, we can find that the major difference between Ricean and Rayleigh channel is the main path (the sight way). In Ricean channel, a main path is defined with the Ricean factor K (the ratio of the power of the direct path to the reflected path) and can be expressed as

$$K = \frac{\rho_0^2}{\sum_{i=1}^{20} \rho_i^2} \quad (3-3)$$

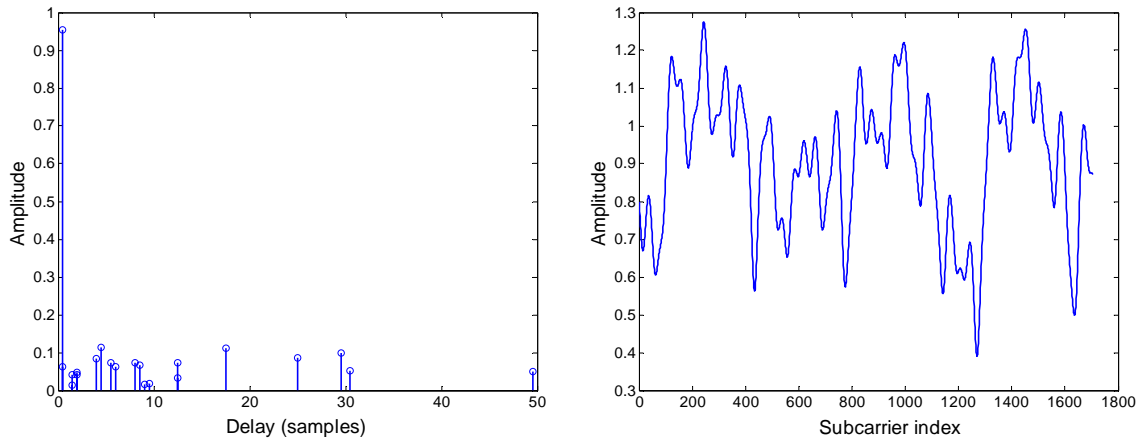
However, there is no main path in Rayleigh channel. Hence the received signals consist of several reflected signals with similar power and bring serious synchronization error. The impulse response and frequency response of the two types of channel when $K=10\text{dB}$ are shown in Fig. 3.5. As we can see there is a significant direct path in the impulse response of the Ricean channel. In the impulse response of the Rayleigh channel, there is no any direct path and all the paths have similar magnitude. Therefore, the frequency selective fading effect in the frequency response of the Rayleigh channel is more serious than that of the Ricean channel.



(a) Impulse response of Rayleigh channel



(b) Frequency response of Rayleigh channel



(c) Impulse response of Ricean channel (d) Frequency response of Ricean channel

Fig. 3.5 Channel response of Rayleigh and Ricean (K=10dB) channel

3.2.2 Doppler Spread Model

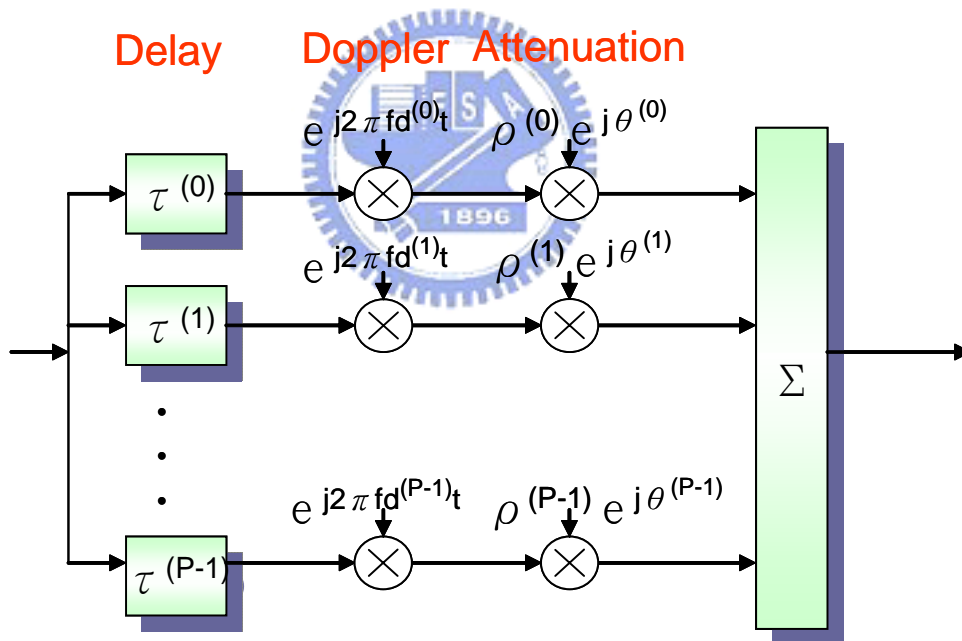


Fig. 3.6 Doppler spread model

In DVB-T/H system, the reception ability in mobile environment is necessary. Hence a mobile radio channel including Doppler spread must be constructed. A simplified Doppler spread model is shown in Fig. 3.6 [22]. In the beginning, we assume a channel with a known and fixed number of paths P such as Rayleigh or Ricean with a Doppler frequency $f_d^{(k)}$,

attenuation $\rho^{(k)} e^{j\theta^{(k)}}$, and time delay $\tau^{(k)}$. All the parameters are fixed as described in section 3.2.1 except the Doppler frequency. Since each path has its own Doppler frequency, the decision of the statistic distribution of f_d is very important. There are two commonly used Doppler frequency PDFs, uniform and classical, where the former exploits uniform distribution to model Doppler spread, and the later uses Jake's Doppler spectrum [23], respectively. The PDF of the Jake's Doppler spread can be expressed as

$$p(f_d) = \frac{1}{\pi \cdot f_{d\max} \cdot \sqrt{1 - \left(\frac{f_d}{f_{d\max}}\right)^2}}, \quad \text{where } |f_d| \leq f_{d\max} \quad (3-4)$$

After transformation of random variable, each f_d can be obtained by the following equation

$$f_d = \cos(2\pi \cdot \text{rand}(1)) \cdot f_{d\max} \quad (3-5)$$

The type of Doppler spread (uniform or Jake's) affects the system performance enormously. Because each path gets different f_d in each simulation case with different $f_{d\max}$, the value of $f_{d\max}$ should be fixed for each simulation and comparison.

3.2.3 Carrier Frequency Offset and Sampling Clock Offset model

The detailed signal model of CFO is already described in section 2.1.1 and will not be discussed repeatedly in this section. The model of SCO is built based on the concept of sinc interpolation. The input digital signals can be exploited to interpolate the intermediate value between two successive samples by using the shifted value of sic function. Assume that the sampling period is T_s and SCO is ζ . Then the sampling phase can be represented as $nT_s + n\zeta$. The resulting signal after ADC can be expressed as

$$\begin{aligned} r_{ADC}(nT_s) &= r(nT_s) * \text{sinc}\left(\frac{nT_s + n\zeta}{T_s}\right) \\ &= \sum_{k=-N}^N r(nT_s - kT_s) \cdot \text{sinc}\left(k + \frac{n\zeta}{T_s}\right) \end{aligned} \quad (3-6)$$

where $2N+1$ is the taps of the FIR interpolator, k is the sampling point index, $r(\cdot)$ is the

received signal with perfect sampling, $r_{ADC}(\cdot)$ is the received signal while SCO is ζ , respectively.

3.3 Performance Analysis

The performance analysis of the proposed CFO synchronization scheme is illustrated in this section. Except the verification of the proposed algorithms, some performance or computational complexity comparison between the conventional and the proposed approach is also made. Finally, the influence of the proposed CFO synchronization scheme to the overall system performance is presented.

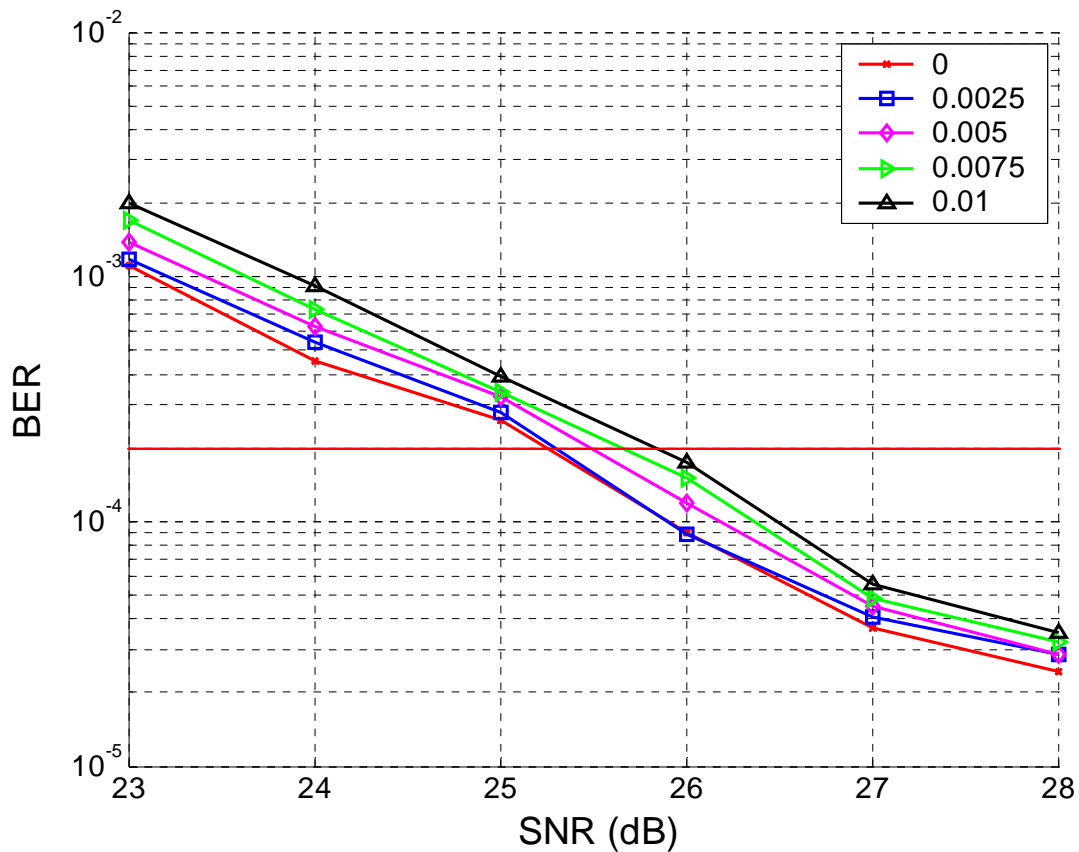


Fig. 3.7 BER performance in different CFO error

In order to measure the estimator performance of the proposed CFO synchronization scheme, the tolerance ability to residual CFO error of the overall DVB-T/H system is measured as shown in Fig. 3.7. The simulation environment is 2k mode, GI=1/8, 64-QAM,

code rate=2/3, and Rayleigh fading channel without Doppler spread and SCO effect. The overall system performance is measured with the BER at Viterbi decoder output is equal to 2×10^{-4} while different residual fractional CFO error occurs without compensation. We can find that when the residual CFO error is less than 0.0025, the system performance degradation is only 0.05dB and not very apparent. However, as the residual CFO error increases to 0.005 and 0.0075, the SNR loss is about 0.2dB and 0.4dB, respectively. Once the residual fractional CFO reaches 0.01, the SNR loss is up to 0.6dB. Therefore, the objective of the CFO synchronization is to make the residual CFO value less than 0.005 after one-shot acquisition and long time tracking to minimize the performance loss of the overall system.

3.3.1 Fractional Carrier Frequency Offset Synchronization

As section 2.3 mentioned, the guard interval based fractional CFO estimation algorithm is very sensitive to the noise introduced by inter-symbol interference (ISI) in deep delay spread channel environment. In particular, the influence of multipath spread is more apparent when the length of guard-interval is shorter. As Fig. 3.5(a) shows, the impulse response of the Rayleigh channel still has two large delay paths near the 30-th sample. If the guard interval length is 1/32 in 2k mode, there are only 64 samples within the guard interval and almost half of them are distorted by the Rayleigh channel spread. Thus the estimator performance of the guard interval based algorithm degrades apparently in such condition. Fig. 3.8 shows the root mean square error (RMSE) performance of the conventional fractional CFO estimator in different guard interval length condition when all signal within guard interval are utilized for estimation. The simulation environment is 2k mode, 64-QAM, code rate=2/3, CFO=0.33 subcarrier space (2.94ppm), and Rayleigh fading channel without Doppler spread and SCO effect. As we can see from Fig. 3.8, the required SNR when RMSE is equal to 0.005 is only about 4dB when guard interval length is 1/4 of the symbol length. However, as guard interval length decreases, the required SNR for 0.005 RMSE increases obviously. The RMSE even

saturates near 0.01 when the guard interval length is 1/32 of the symbol length. In order to improve the performance of the guard interval based fractional CFO estimator, the ISI noise must be reduced by discarding some samples of the guard interval.

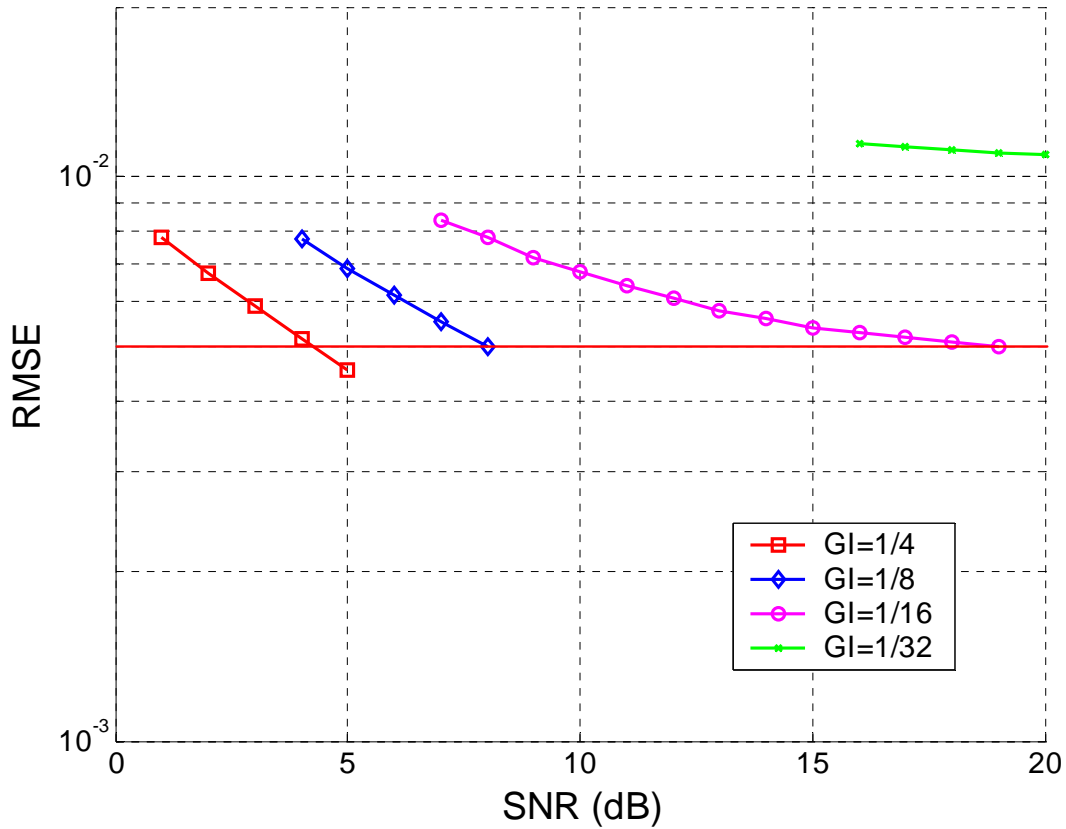


Fig. 3.8 RMSE performance in different guard interval length

As previous mentioned the ISI noise caused by multipath delay spread degrades the performance of fractional CFO estimator apparently. Therefore in our proposed fractional CFO acquisition algorithm, the first y samples of guard interval are skipped during calculating the correlation of the cyclic prefix. The number of skipped samples y should be chosen carefully according to the multipath channel environment. In long delay spread condition, y should be chosen as large as possible to avoid the ISI distortion. However, if a large y is chosen, the remaining samples within guard interval for correlation may be too few to average the AWGN noise in short guard interval condition. For example, there are only 64 samples within the guard interval while 1/32 guard interval length in 2k mode, if the y is chosen larger

than 40, the number of remaining samples is less than 24 and can not average the AWGN noise effectively. In order to choose an appreciate value of y for different guard interval length spec among various channel condition, the most critical condition which includes 1/32 guard interval length in 2k mode and Rayleigh fading channel is considered and simulated as Fig. 3.9 shows. The simulation environment is 2k mode, GI=1/32, 64-QAM, code rate=2/3, CFO=0.33, and Rayleigh fading channel without Doppler spread and SCO effect. From Fig.3.9 we can see that as y increases, the RMSE of the estimator can be reduced effectively and achieves the 0.005 target when $y=30$ at 18.3 dB SNR. However, if y is chosen as 35, the remaining samples for correlation will be less than 29 and can not average the AWGN noise in low SNR environment effectively. So in our proposed fractional CFO acquisition algorithm, y is chosen as 30 to improve the estimator performance.

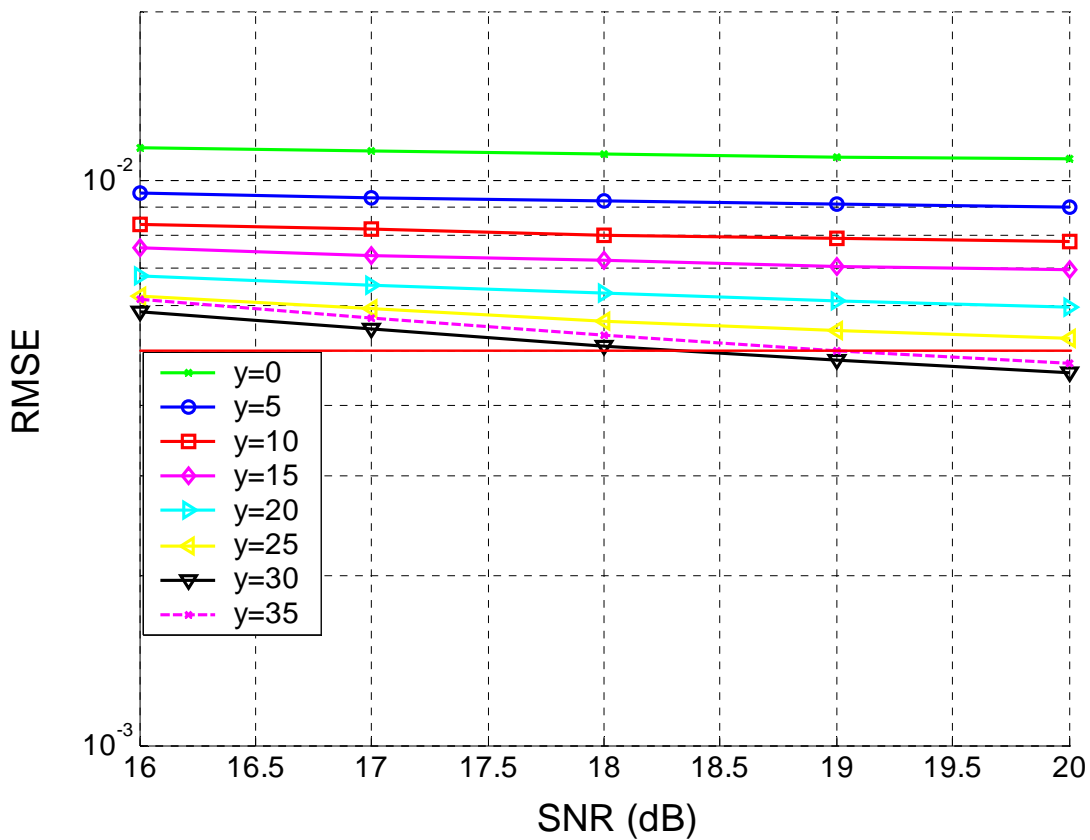


Fig. 3.9 RMSE performance in different y

The RMSE performance comparison between the conventional and the proposed

fractional CFO acquisition is shown in Fig. 3.10. The improved SNR while RMSE is 0.005 is also listed in Table 3.1. The simulation environment is 2k mode, 64-QAM, code rate=2/3, CFO=-0.33, and Rayleigh fading channel without Doppler spread and SCO effect. As we can see the RMSE performance improvement is the most apparent when the guard interval length is the shortest. And the simulation result also proves that the proposed algorithm can eliminate ISI noise effectively.

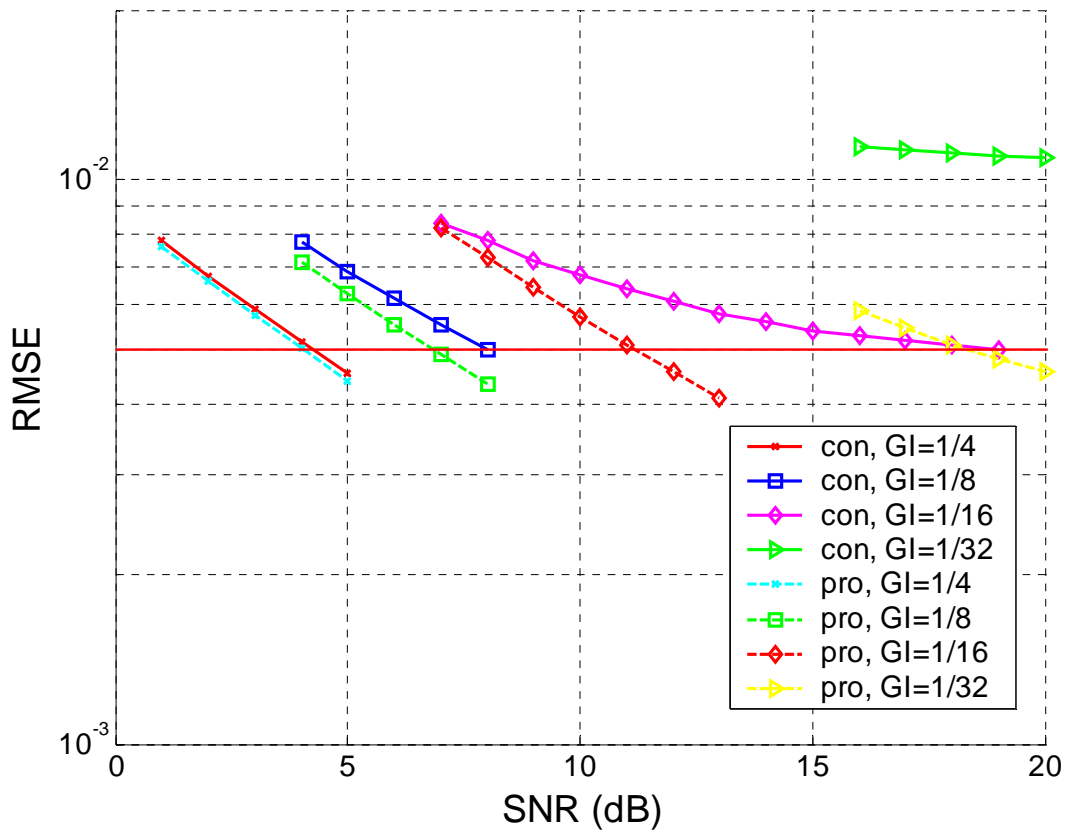


Fig. 3.10 RMSE performance comparison

Table 3-1 Performance comparison of fractional CFO estimator

	1/4	1/8	1/16	1/32
Conventional	4.25	7.8	19	N.A.
Proposed	4	6.8	11.2	18.5
Improved SNR	0.25	1	7.8	N.A.

3.3.2 Integral Carrier Frequency Offset Synchronization

In order to acquire correct subcarrier index for the following channel estimator and TPS decoder, the estimation result of the integral CFO acquisition must be accurate perfectly. Hence the estimation failure rate is used for evaluating the performance of the integral CFO synchronization. In our integral CFO synchronization scheme, the integral CFO estimator is composed of 2 stages, where the first stage detects whether the integral CFO is positive or negative, and the second stage finds the accurate integral CFO value, respectively. Both of the two stages should achieve acceptable performance even in critical channel condition to acquire accurate estimation result. We will analysis the performance of the two stages, and then illustrate the overall estimator performance and make some comparison with conventional algorithms in order.

The first stage of the proposed integral CFO estimator utilizes both sides of the boundary between data and guard band subcarriers as searching window to detect the shift direction caused by integral CFO. Hence the window width w_1 is the most important parameter of this stage. A wider window width can achieve better performance in low SNR condition but leads to more number of multiplication. The trade-off between estimation performance and computational complexity should be decided and simulated as Fig. 3.11 shows. The simulation environment is 2k mode, GI=1/8, 64-QAM, code rate=2/3, CFO=10 (89.2ppm), and Rayleigh fading channel without Doppler spread and SCO effect. The estimation failure rate is acquired by applying 1200 OFDM symbols for simulation and then calculating the ratio of the number of failure estimation to total number of simulated symbols. As we can see from Fig. 3.11, when the target estimation failure rate is set as 0.001, the window width which is equal to 5 can satisfy both target estimation performance at 8.8dB SNR and lower computational complexity at the same time. Therefore, the window width w_1 of the first stage of the proposed integral CFO acquisition is chosen as 5 in the future simulation results.

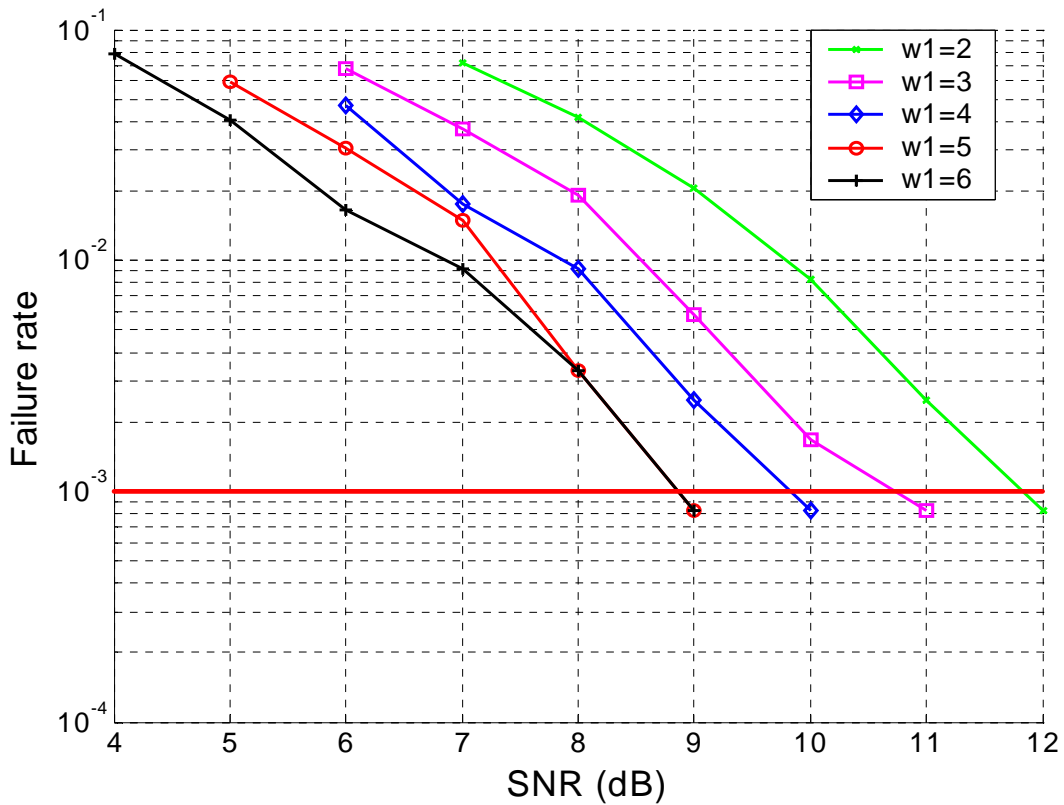


Fig. 3.11 Performance of the first stage with different window width

Fig. 3.12 shows the performance of the first stage of the proposed integral CFO estimator in different channel models. The simulation environment is 2k mode, GI=1/8, 64-QAM, code rate=2/3, CFO=10, and SCO=0ppm. The simulated channel models are Gaussian channel, Ricean channel, static Rayleigh channel, and mobile Rayleigh channel, respectively. From Fig. 3.12 we can see that when the estimation failure rate is equal to 0.001, the SNR loss of Ricean channel is only 1dB compared with the AWGN only condition because the frequency selective fading effect of the Ricean channel is relatively weaker than that of the Rayleigh channel as Fig. 3.5 shows. In the case of mobile Rayleigh channel, the maximum Doppler frequency is chosen as 70Hz which is corresponding to velocity of 150km/h to achieve practical mobile situation. As we can see the SNR loss caused by Doppler spread compared with the static Rayleigh channel is about 4dB. Hence the time-varying frequency selective fading affects the estimator performance obviously.

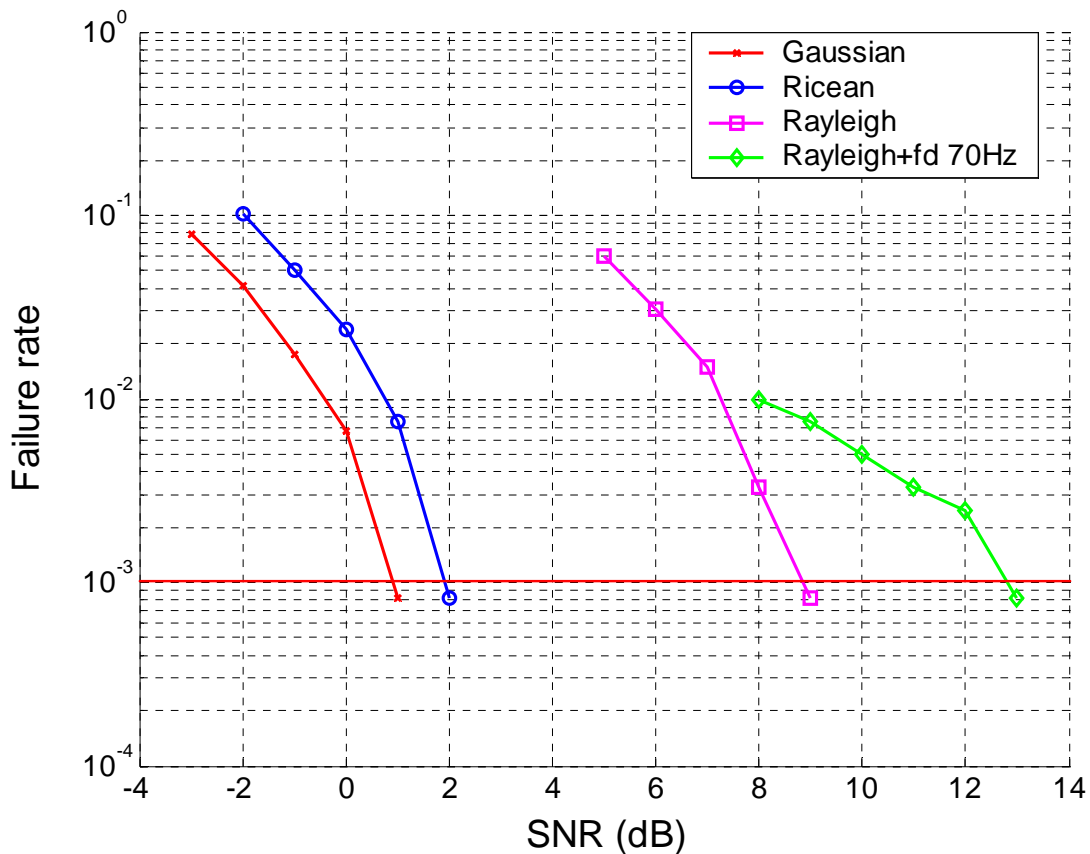


Fig. 3.12 Performance of the first stage in different channel models

In the second stage, two algorithms are proposed for searching the shift index caused by integral CFO according to the direction detected by the first stage. The first algorithm is based on the reduced number of continual pilots. The number of correlated continual pilots affects the estimation performance and computational complexity directly. Fig. 3.13 shows the estimator performance of the proposed reduced continual pilots approach while correlating different number of pilots. The simulation environment is 2k mode, GI=1/8, 64-QAM, code rate=2/3, CFO=10, and Rayleigh fading channel without Doppler spread and SCO effect. As we can see, the number of correlated continual pilots can be chosen as 15 to provide error-free estimation when SNR is larger than 4dB and consume about only 1/3 number of multiplication compared with the conventional continual pilots based algorithm which correlates all 45 continual pilots.

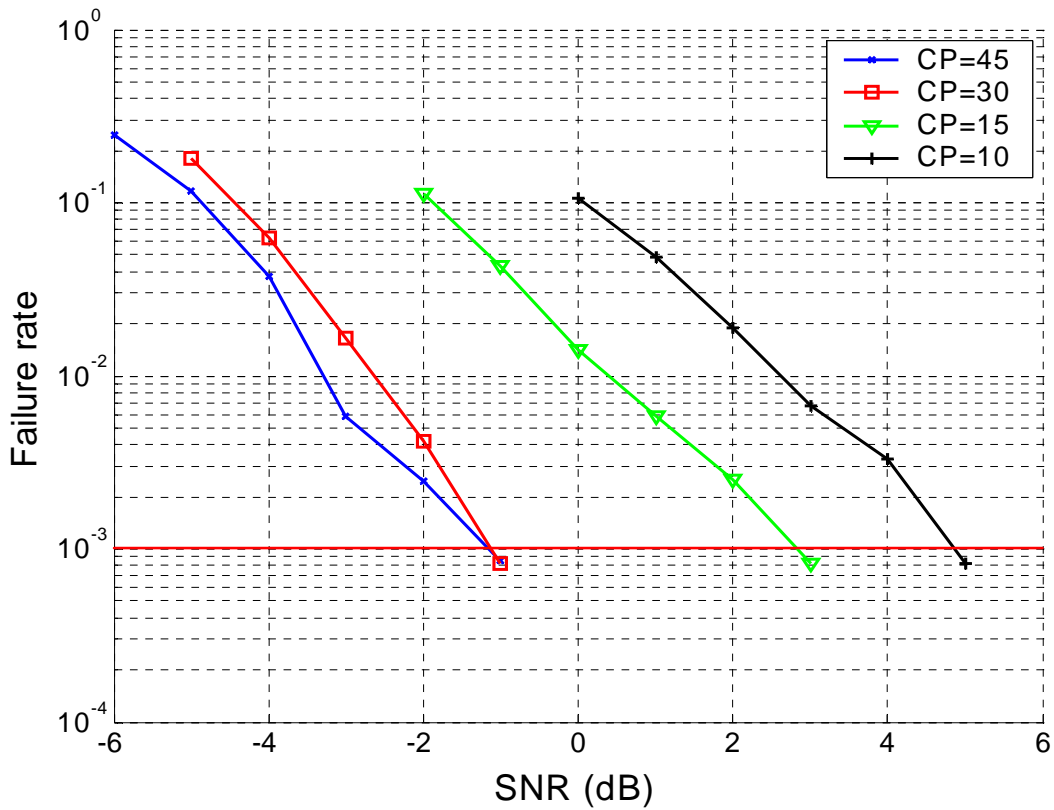


Fig. 3.13 Continual pilots based approach with different number of pilots

The other proposed algorithm for the second stage of the integral CFO acquisition is based on the guard band moving window algorithm. Similar to the first stage, the moving window width w_2 is an important parameter of this algorithm. Fig. 3.14 shows the estimator performance of the proposed guard band based algorithm for the second stage with different moving window width. The simulation environment is 2k mode, GI=1/8, 64-QAM, code rate=2/3, CFO=10, and Rayleigh fading channel without Doppler spread and SCO effect. As we can see the window width can be chosen as 10 to provide error-free estimation while SNR is larger than 15dB in Rayleigh fading channel. If the constellation mode is simpler such as QPSK in Rayleigh channel, the required SNR for quasi error-free condition (BER after Viterbi decoder is equal to 2×10^{-4}) may be near the required error-free SNR of the proposed guard band based approach. Therefore we must check the result of scatter pilot mode detector or TPS decoder to assure the estimation result of this algorithm is correct in such condition.

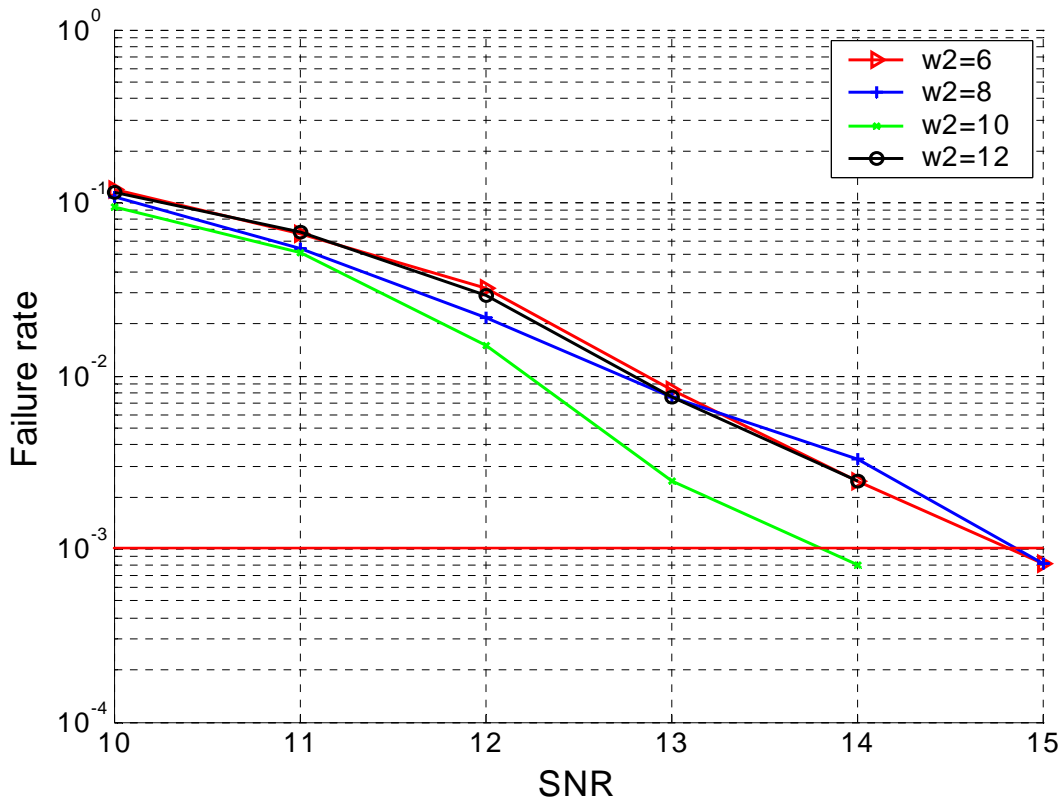


Fig. 3.14 Proposed guard band based approach with different window width

In order to evaluate the performance of the proposed integral CFO estimator, the two stages should be combined together in the later simulation results. The related parameters of the proposed integral CFO estimator are shown in Table 3-2.

Table 3-2 Parameters of the proposed integral CFO estimator

Search range m	60
Window size of Con GB w	5
Window width of the first stage w_1	5
Window width of the second stage w_2	10
Index of the 15 correlated continual pilots in Pro CP	0 48 141 255 282 432 531 759 918 942 1101 1110 1140 1323 1704

The performance comparison between the conventional and the proposed integral CFO estimators will be illustrated in different channel conditions. Fig. 3.15 shows the performance of the two conventional and two proposed integral CFO estimators in Gaussian channel model. The simulation environment is 2k mode, GI=1/8, 64-QAM, code rate=2/3, CFO=10, $f_d=0$ Hz, and SCO=0ppm. Where the Con indicates the conventional, Pro is the proposed, GB is the guard band based, and CP is the continual pilots based, respectively. As we can see the conventional continual pilots based approach requires the lowest SNR for 0.001 estimation failure rate. However, the number of multiplication of this algorithm is also the largest among the four approaches. The proposed continual pilots based algorithm is about 6dB higher but consumes much lower computational complexity than the conventional continual pilots based one. As for the two guard band based algorithms, the proposed one achieves about 2dB lower than the conventional one because of its three symbols summation scheme.

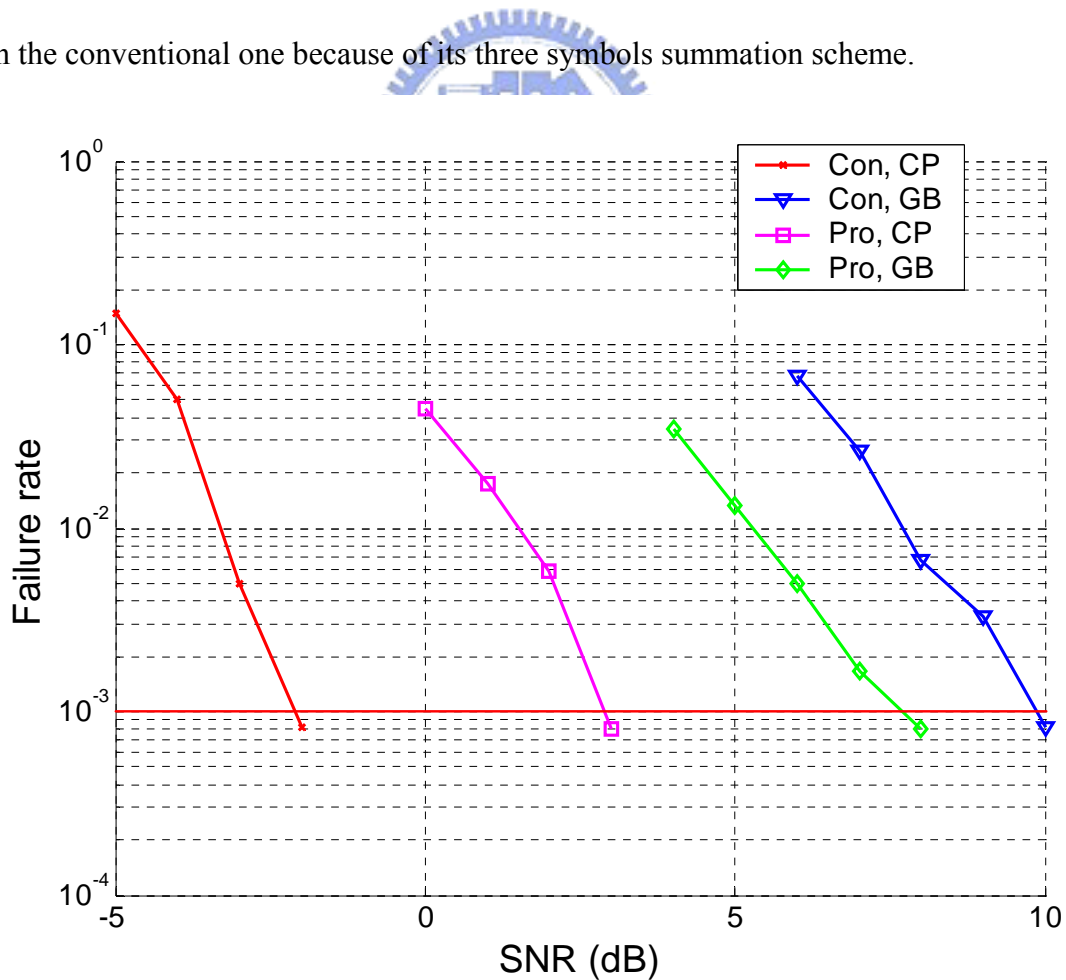


Fig. 3.15 Performance of different integral CFO estimators in Gaussian channel

Fig. 3.16 shows the performance comparison in Ricean channel model ($K=10\text{dB}$). The simulation environment is 2k mode, $GI=1/8$, 64-QAM, code rate= $2/3$, $CFO=10$, $f_d=0\text{Hz}$, and $SCO=0\text{ppm}$, respectively. We can find that the simulation result is very similar to that in Gaussian channel because the Ricean channel model has a main path which leads to flatter channel frequency response in frequency domain. The required SNR for 0.001 estimation failure rate is also in inverse proportion to the number of multiplication.

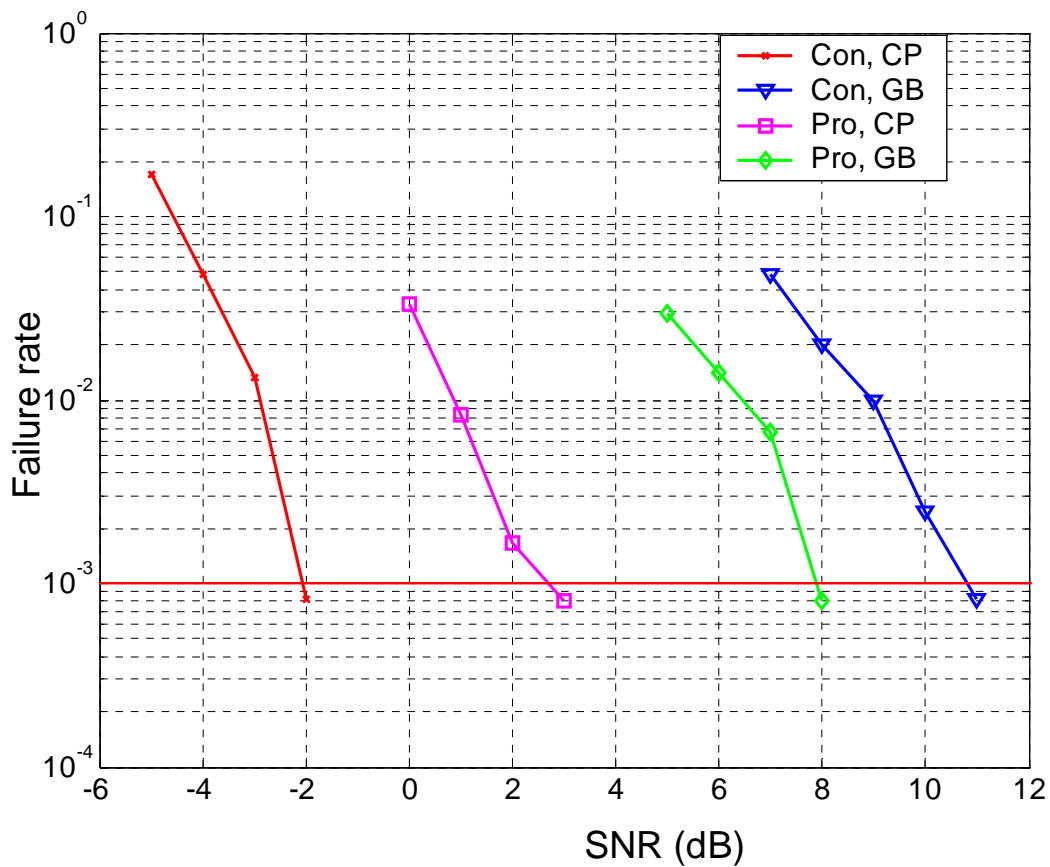


Fig. 3.16 Performance of different integral CFO estimators in Ricean channel

The performance comparison among the four integral CFO estimators in static Rayleigh channel is shown in Fig. 3.17. The simulation environment is 2k mode, $GI=1/8$, 64-QAM, code rate= $2/3$, $CFO=10$, $f_d=0\text{Hz}$, and $SCO=0\text{ppm}$, respectively. Because the serious frequency selective fading effect caused by the Rayleigh channel model distorts the signals in frequency domain, the required SNR for 0.001 failure rate increases apparently except the conventional continual pilots based approach due to its high computational complexity. Compared with Fig.

3.13, the performance of the proposed continual pilots based approach degrades because the first stage performs worse than the second stage in static Rayleigh channel model. Hence the performance of the proposed two stage scheme is dominated by the stage which performs worse than the other one.

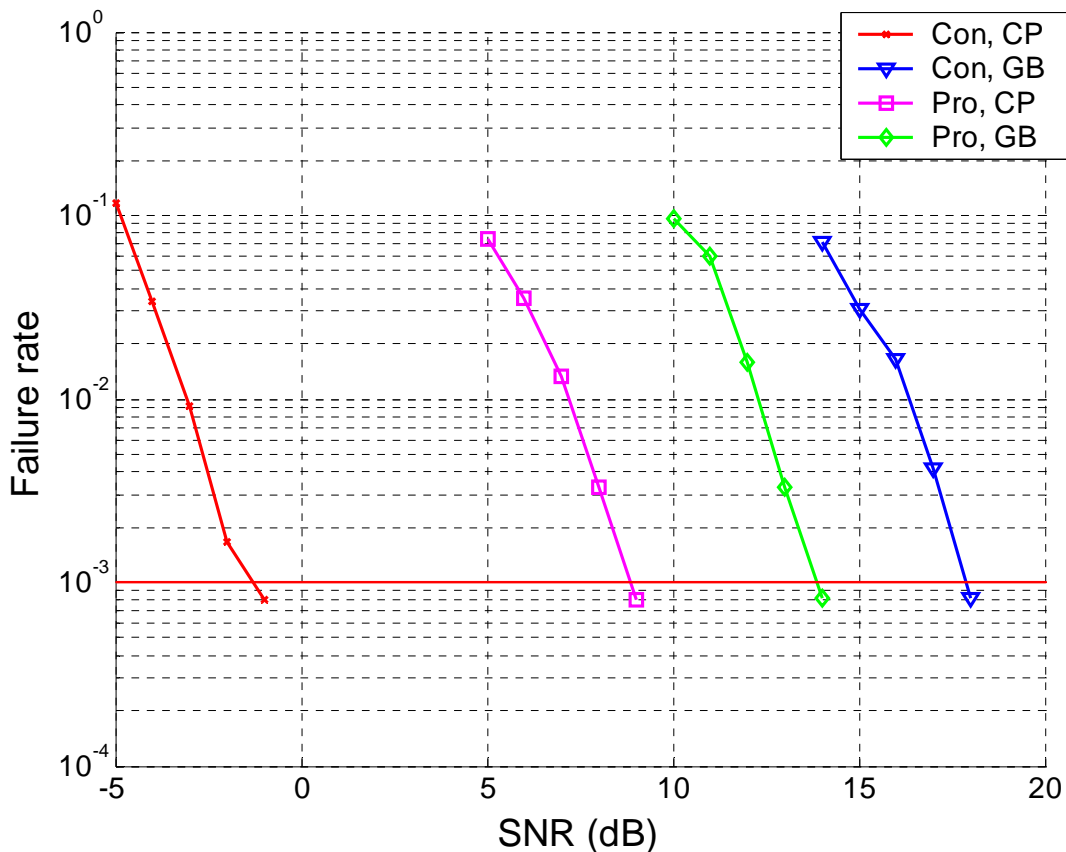


Fig. 3.17 Performance of different integral CFO estimators in static Rayleigh channel

As for time-varying environment, the performance comparison among the four integral CFO estimators in mobile Rayleigh channel is shown in Fig. 3.18. The simulation environment is 2k mode, GI=1/8, 64-QAM, code rate=2/3, CFO=10, $f_d=70\text{Hz}$, and SCO=0ppm, respectively. As we can see in mobile environment, the frequency selective fading effect becomes time-varying and brings more distortion to the signals in frequency domain than the time-invariant condition. The error-free SNR of the conventional guard band based approach even exceeds 30dB and degrades about 15dB compared with the static Rayleigh channel. The conventional continual pilots based algorithm still keeps the lowest

error-free SNR as the previous simulation results. The performance degradation of the two proposed algorithms due to time-varying Rayleigh channel is not as serious as the conventional guard band based algorithm.

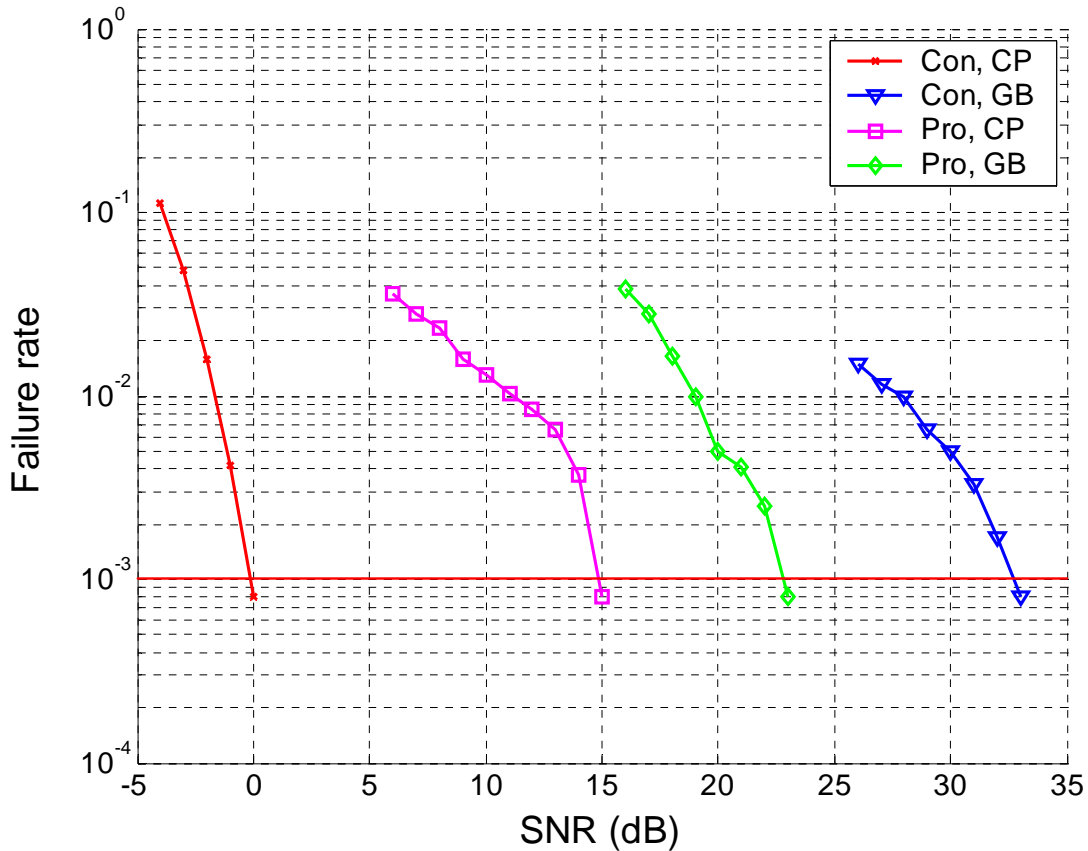


Fig. 3.18 Performance of different integral CFO estimators in mobile Rayleigh channel

From above simulation results we can see that the computational complexity affects the performance of the integral CFO estimator directly. The more number of multiplication is utilized, the lower error-free SNR is achieved. The number of multiplication of the four algorithms in 2k mode according to the simulation parameters which is shown in Table 3-2 is listed in Table 3-3. As we can see although the conventional continual pilots based approach requires the lowest SNR in various channel condition, it consumes much more number of multiplication than the other three algorithms. Because the difference between the quasi error-free SNR of the overall system and the error-free SNR of the conventional continual pilots based algorithm is very large, it is not necessary to consume such huge computational

complexity by exploiting this approach. If the most economical conventional guard band based approach is utilized, its error-free SNR is even larger than the quasi error-free SNR of the system in QPSK constellation when the channel model is more critical such as Rayleigh channel. Therefore, considering the trade-off between computational complexity and estimator performance, the proposed two algorithms may be better solutions to balance it.

Table 3-3 Number of multiplication comparison

	Con, CP	Con, GB	Pro, CP	Pro, GB
# of multiplication	22022	500	4132	940
scale	100%	2.28%	18.76%	4.27%

3.3.3 Residual Carrier Frequency Offset Tracking

The residual CFO tracking of the proposed CFO synchronization scheme is composed of a one-shot residual CFO estimator followed by a PI loop filter as mentioned in chapter 2. In this section, we will discuss the performance of the one-shot residual CFO estimator first. Unlike the fine CFO estimator, the residual CFO estimator should not be affected by the guard interval length or multipath delay spread easily to assure lower estimation error. So in our proposed residual CFO estimation scheme, the continual pilots based algorithm is exploited. The RMSE performance of the residual CFO estimator in various channel models is simulated and shown in Fig. 3.19. The simulation environment is 2k mode, GI=1/8, 64-QAM, code rate=2/3, residual CFO=0.02 (0.178ppm), and SCO=0ppm, respectively. From the simulation we can see that the RMSE performance is almost the same in static channel condition because the average of phase of continual pilots can eliminate the distortion induced by channel frequency response. In the case of time-varying channel when the Rayleigh channel with Doppler frequency 70Hz is applied, the required SNR for 0.005 RMSE degrades about 3dB and is still within acceptable range.

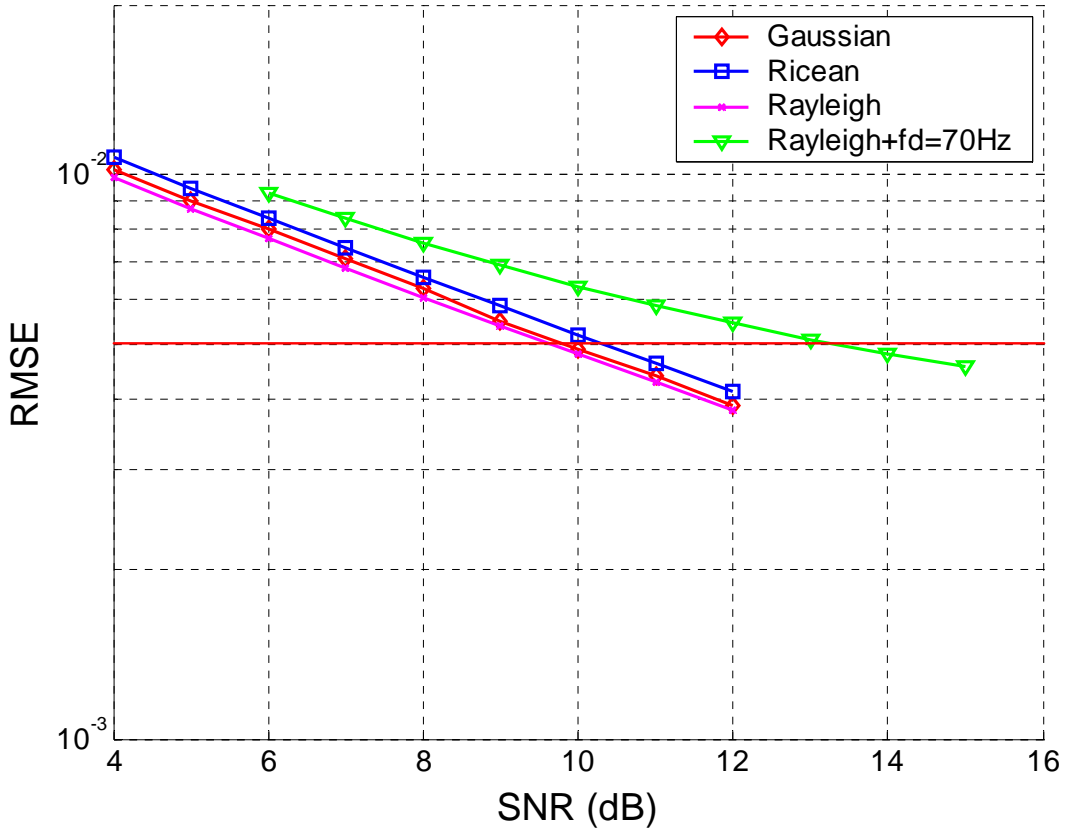


Fig. 3.19 RMSE of one-shot residual CFO estimator in different channel models

The objective of the PI loop filter is to reduce the variance of the estimated residual CFO value from previous stage. In order to reduce the hardware complexity, the loop filter parameter is chosen as $K_p = K_i$ in our proposed CFO tracking scheme. As mentioned in chapter 2, the loop filter parameter affects the convergence speed and steady-state standard deviation directly. A larger K_p reduces the convergence time but increases the steady-state standard deviation at the same time. The influence of different loop filter parameters to the residual CFO tracking loop is simulated and shown in Fig. 3.20. The simulation environment is 2k mode, GI=1/8, 64-QAM, code rate=2/3, SNR=15dB, SCO=0ppm, residual CFO=0.02, and Rayleigh channel without Doppler spread, respectively. The total number of simulated symbols is 648. As we can see when a larger K_p is exploited ($K_p = 1/4$), the CFO tracking loop achieves steady-state around 50 symbols and the steady-state standard deviation is 1.8×10^{-3} . However, when a smaller K_p is utilized ($K_p = 1/32$), the convergence time increases to

about 200 symbols but produces smaller steady-state standard deviation which is only 4.73×10^{-4} . In order to achieve both fast convergence speed and low steady-state standard deviation, the loop filter parameter K_p can not be chosen as a fixed value.

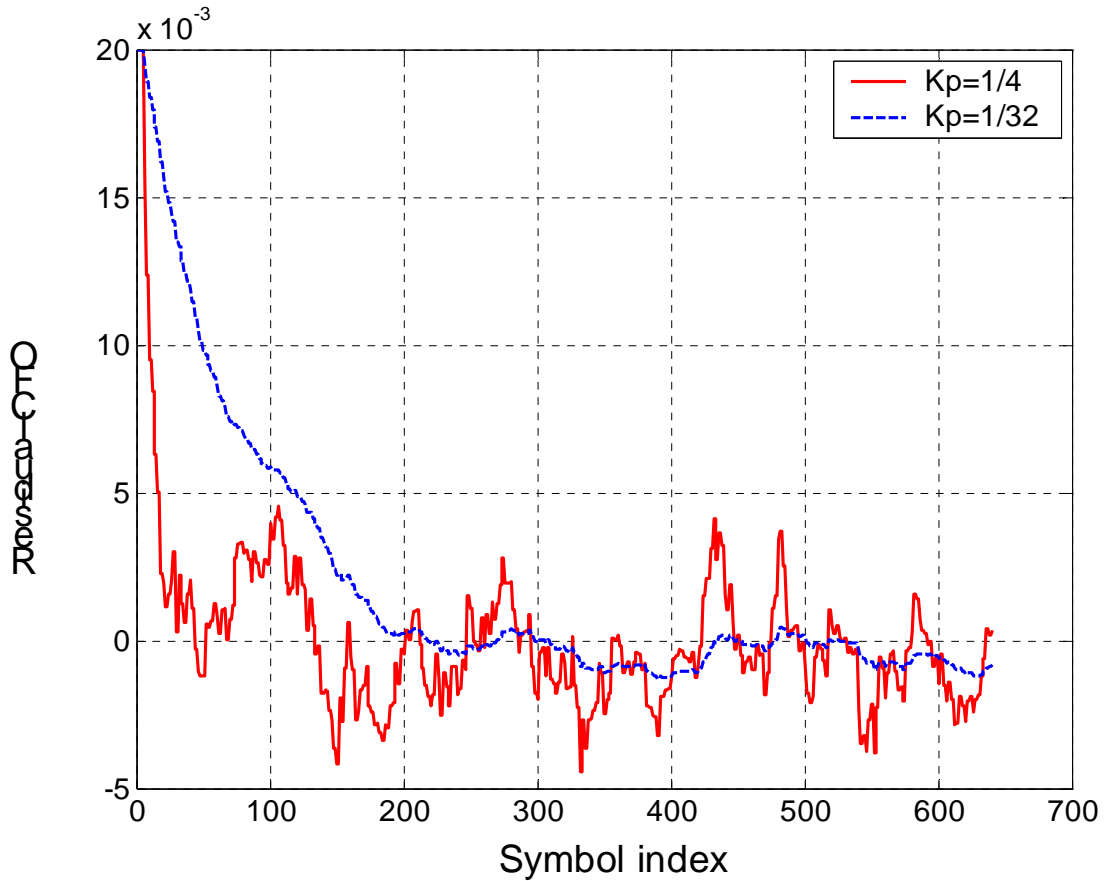


Fig. 3.20 CFO tracking loop in with different parameters

As previously mentioned, the loop filter parameter K_p should be flexible and changed with symbol index to acquire fast convergence speed and lower steady-state standard deviation. Hence a multi-stage residual CFO tracking loop is proposed. A 2-stage and a 3-stage residual CFO tracking loop are exploited and simulated as shown in Fig. 3.21. The simulation environment is the same as Fig. 3.20 except the Doppler spread is 70Hz. As we can see in order to achieve small residual error within a frame (68 symbols), the K_p is chosen as 1/4 for the head 50 symbols, and then changed to 1/32 to acquire lower steady-state standard deviation. If we want to get more accurate tracking result, the 3-stage scheme can change K_p to 1/256 after the 150-th symbol as Fig. 3.21 shows. The steady-state standard

deviation of the 2-stage and 3-stage scheme is 1.5×10^{-3} and 9.41×10^{-4} , respectively. Compared with the simulation result which is shown in Fig. 3.20, we can see that the time-varying channel frequency response degrades the residual CFO tracking loop performance apparently. Therefore the 3-stage residual CFO tracking loop is a better choice for long time reception and mobile environment.

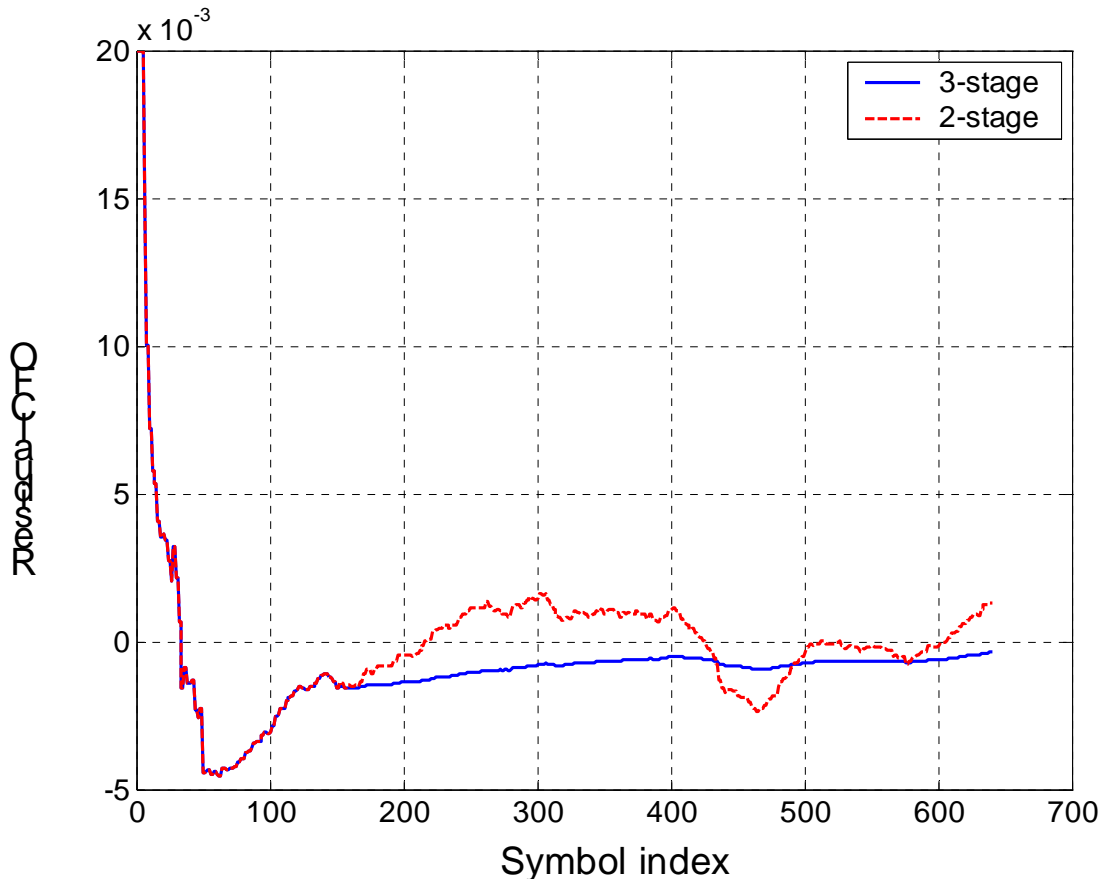


Fig. 3.21 Residual CFO tracking loop with different stage

3.3.4 Overall System Performance

In this section, we will show the performance of the overall system. The quasi-error free condition which corresponds to 2×10^{-4} BER after Viterbi decoder will be the performance target of this section. In order to evaluate the influence of the proposed CFO synchronization scheme to the overall scheme, the most critical operation mode which includes 2k mode and GI=1/32 is considered in the following simulation results. Besides, in the integral CFO

acquisition stage, we exploit the proposed guard band based approach to verify if its performance is acceptable for all kinds of conditions. For separating fixed reception from portable reception, we divide the overall system performance into two parts: static channel and mobile channel.

The overall system performance in three types of static channel model is shown as from Fig. 3.22 to Fig. 3.24. The simulation environment is 2k mode, GI=1/32, code rate=2/3, SCO=20ppm, and CFO=10.33 (92.14ppm), respectively. The solid line means the synchronization of CFO is perfect, and the dashed line means the result that utilizes the proposed CFO synchronization scheme. As we can see the frequency selective fading of multipath channel brings unavoidable performance degradation compared with the AWGN condition. Compared with the AWGN channel, the SNR loss of ideal case is about 2dB in Ricean channel and 8dB in Rayleigh channel.

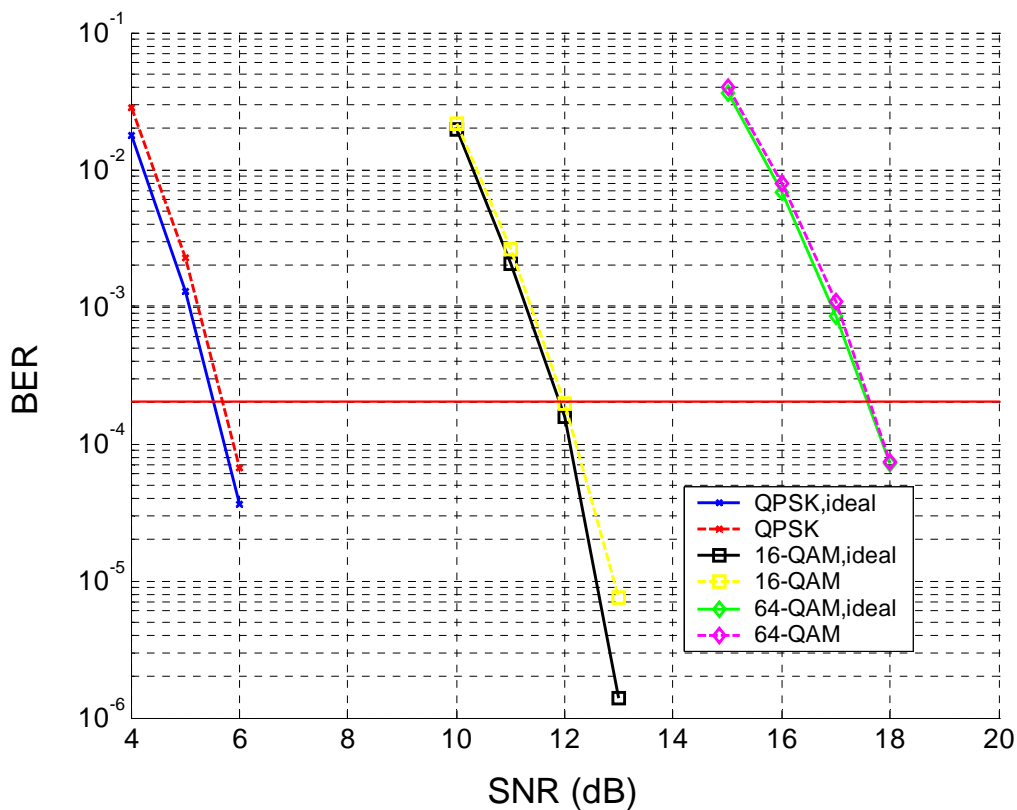


Fig. 3.22 Overall system performance in Gaussian channel

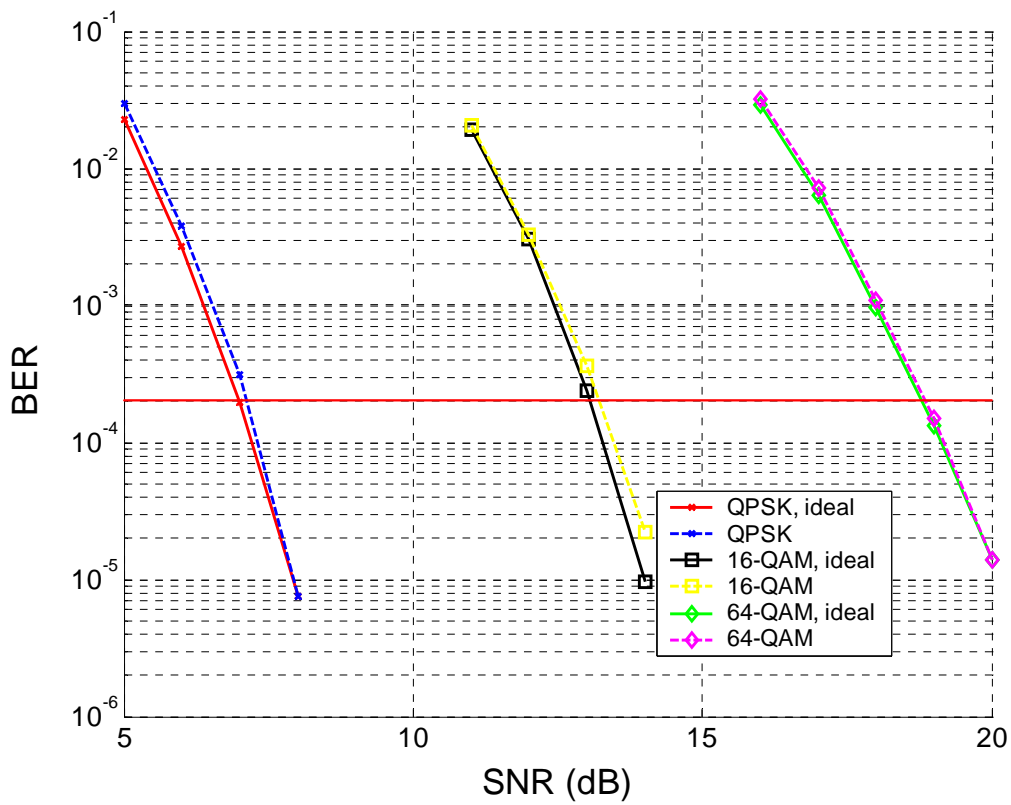


Fig. 3.23 Overall system performance in Ricean channel

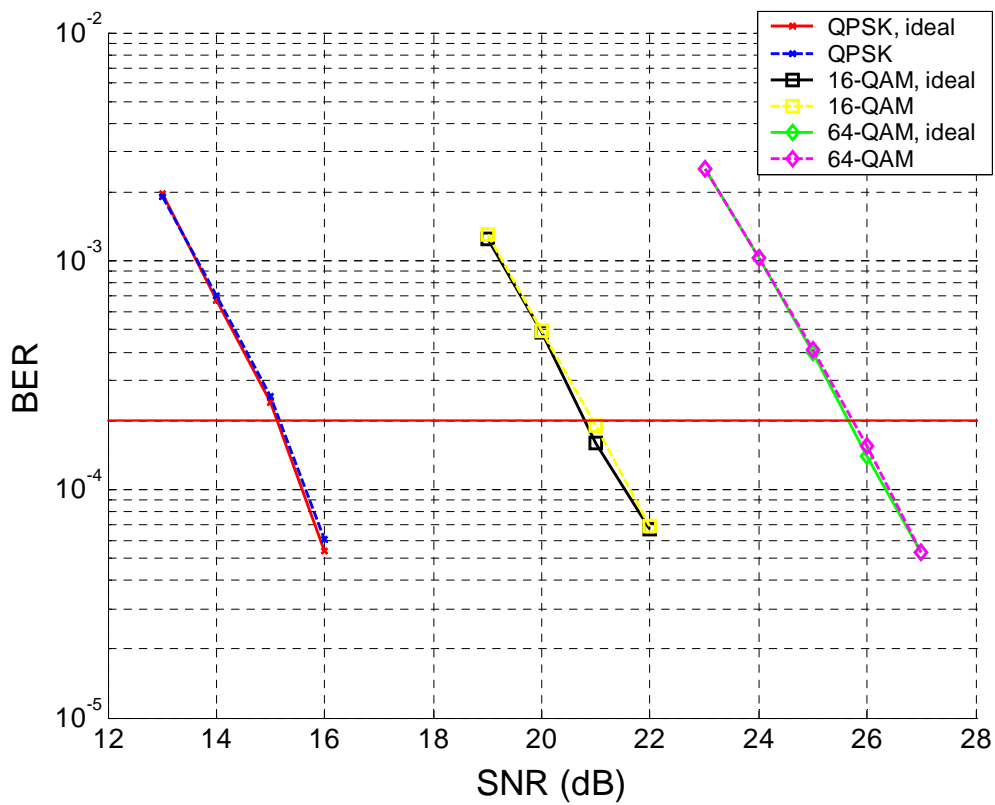


Fig. 3.24 Overall system performance in Rayleigh channel

The overall system performance in mobile channel is evaluated and simulated as shown in Fig. 3.25. The simulation environment is 2k mode, GI=1/32, code rate=2/3, SCO=20ppm, CFO=10.33, and Rayleigh channel with Doppler spread 70Hz, respectively. We can see that the performance degradation of the time-varying channel is more serious than the static condition. Compared with the AWGN channel, the SNR loss of ideal case is about 10dB in mobile Rayleigh channel. The SNR loss due to the proposed CFO synchronization scheme is as shown in Table 3-4.

Table 3-4 SNR loss due to synchronization in different channel models

	Gaussian	Ricean	Rayleigh	Rayleigh+f _d =70Hz
QPSK	0.17	0.12	0.07	0.20
16-QAM	0.08	0.15	0.18	0.08
64-QAM	0.03	0.08	0.10	0.10

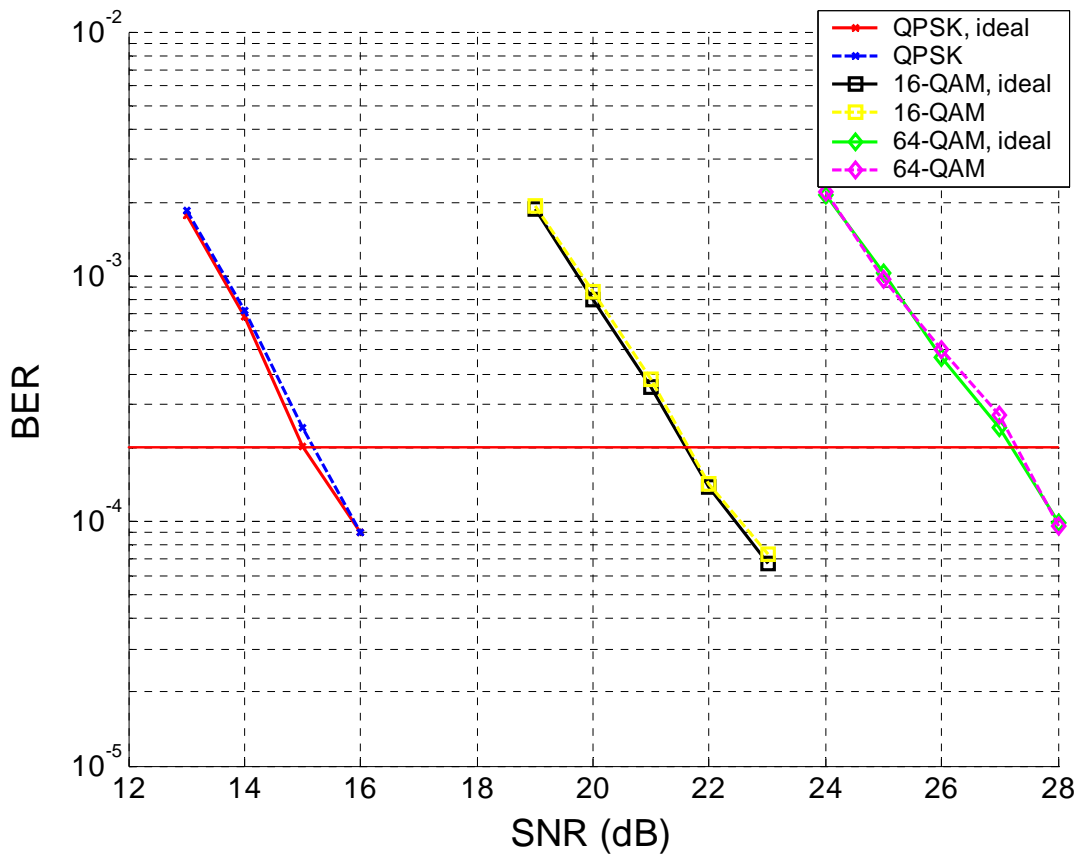


Fig. 3.25 Overall system performance in mobile Rayleigh channel

Chapter 4 .

Architecture and Implementation

In this chapter, the platform based design methodology will be introduced first. Then the architecture of the implemented DVB-T/H receiver will be illustrated. The architecture of the proposed CFO synchronization design, hardware synthesis information and chip summary will be shown in the following sections.

4.1 Design Methodology

The trend of IC technology is towards to System-on-Chip (SoC). System-level simulation becomes very important in today's design flow. Our design methodology from system simulation to hardware implementation can be shown in Fig. 4.1. First, the system platform and channel modals should be established according to the system specification with MATLAB language, which ensures the design in the practical condition. Algorithm research and architecture development of each function block should be verified in the system platform to ensure the whole system performance. Fixed-point simulation is applied before hardware implementation to make the trade-off between system performance and hardware cost. In hardware implementation, the Verilog HDL modules are verified with the test benches dumped from the equivalent Matlab blocks to ensure the correctness. Finally, once the verification between HDL modules and fixed-point MATLAB platform is finished, the HDL based platform will be synthesized and translated to circuit level by place and route (P&R) tools.

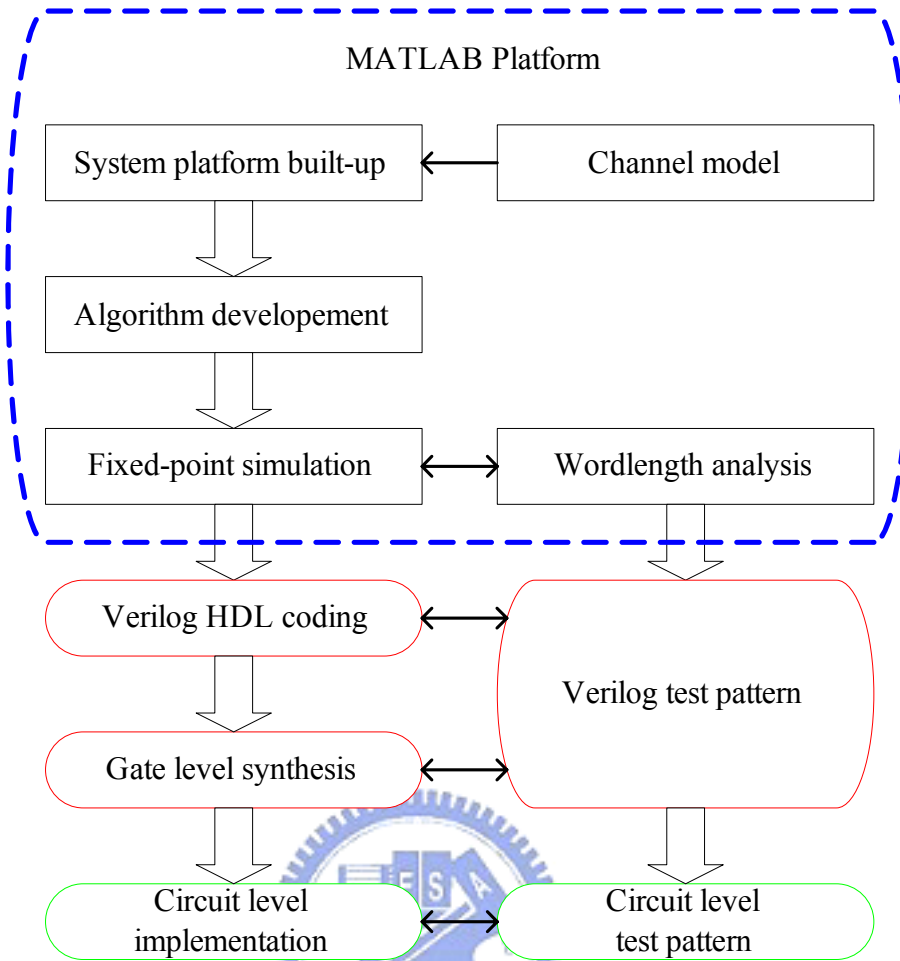


Fig. 4.1 Platform-based design methodology

4.2 Architecture of the DVB-T/H Baseband Receiver

Based on the proposed low complexity CFO synchronization scheme and other low power designs such as high speed FEC decoder and dynamic scheduling FFT processor [24], a DVB-T/H baseband receiver is implemented and tapped out in Jun. 2005. The architecture and corresponding clock rate of the DVB-T/H baseband receiver is shown in Fig. 4.2. As we can see the received data is oversampled at 2 times of the original sampling rate and then interpolated by resampler to recovery sampling clock drift. The clock rate of the main datapath within inner receiver is raised up to four times of the original data rate to meet continuous symbol reception because the required operation time of the FFT processor is about four times of the symbol duration. After the de-QAM constellation, the clock rate is

raised up to six times of the original data rate to satisfy the bit-level calculation. In DVB-T/H system, different channel bandwidths will correspond to different clock rates. The highest clock rate of the received data is about 9MHz when the 8MHz channel bandwidth is utilized. In order to assure that the implemented chip can work in such condition properly, the basic clock rate of the synthesis result is set at 11MHz. The detailed architecture of the proposed CFO synchronization scheme and the chip summary will be illustrated in later sections.



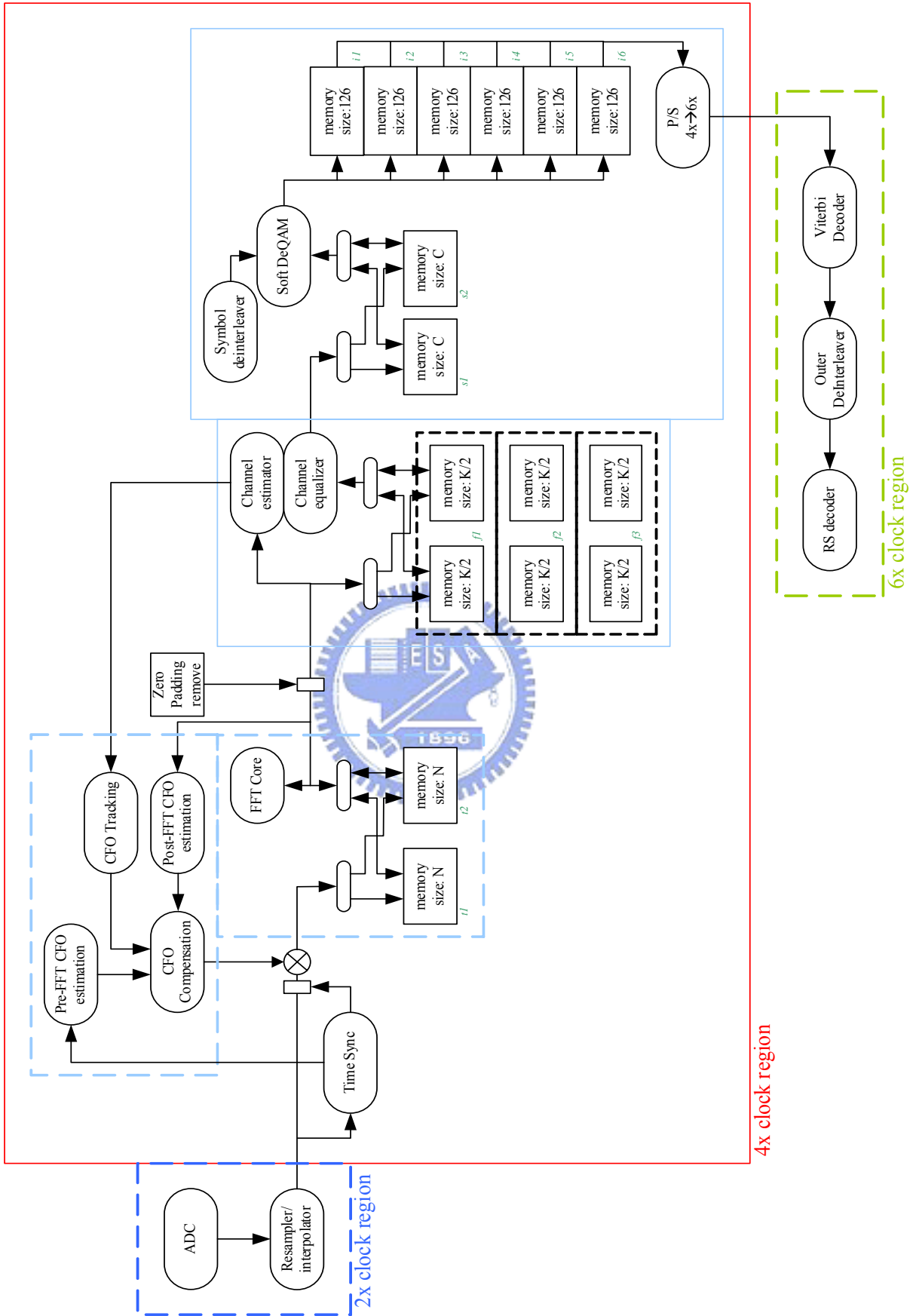


Fig. 4.2 Architecture of the DVB-T/H baseband receiver

4.3 Architecture of Carrier Frequency Offset Synchronization

In this section, the detailed architecture of each functional block of the CFO synchronization scheme will be illustrated. The synthesis result will also be listed based on the implemented DVB-T/H receiver chip which is tapped out in Jun. 2005.

4.3.1 Fractional Carrier Frequency Offset Synchronization

The hardware architecture of the proposed fractional CFO estimator is shown in Fig. 4.3. The correlation between $R_{l,n}$ and $R_{l,n-N}$ is calculated by a complex multiplier and a size N memory. The accumulation length is controlled by the controller based on the number of discarded samples y and the actual length of the guard interval that detected by the mode/GI detector. In our inner receiver design, the coarse symbol synchronization is accomplished by the normalized maximum correlation (NMC) algorithm and exploits the correlation between $R_{l,n}$ and $R_{l,n-N}$, too [21]. The operations would not overlap because the synchronization of symbol bound and fractional CFO are both in acquisition stage. Hence the complex multiplier and size N memory can be combined with the coarse symbol synchronizer together.

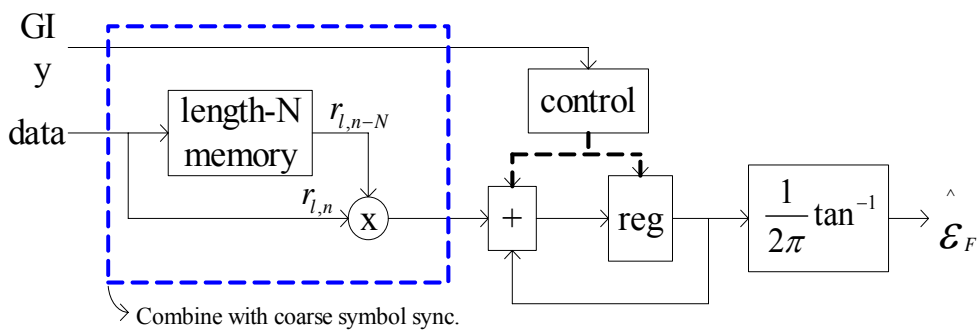


Fig. 4.3 Architecture of fractional CFO estimator

The objective of the arc-tangent component is to calculate the phase of the complex correlation result. In our proposed fine CFO estimator, the arc-tangent component is combined with the constant multiplier that multiplies the calculated phase value by $1/2\pi$ to

save the additional hardware resource for the constant multiplication. The architecture of the conventional arc-tangent approaches can be divided into a direct-TLU method and a division-based TLU method [25]. The former requires a large look-up table when the input wordlength is longer, and the later consumes a divider that costs large hardware area and long latency, respectively. Hence in our proposed fractional CFO estimator, a logarithm-based TLU arc-tangent method is utilized for the phase calculation to achieve low power and high speed consideration [26]. By adopting this technique, the size of look-up table can be reduced effectively and a division free architecture can be obtained by using only combinational addition and subtraction. The synthesis result of the proposed fine CFO estimator in a 0.18 μ m cell library with clock rate equals to 11MHz is shown in Table 4-1.

Table 4-1 Synthesis result of the fractional CFO estimator

	Gate Count
Combinational	11260
Non-Combinational	692
Total	11952

4.3.2 Integral Carrier Frequency Offset Synchronization

In order to achieve low power consideration, the proposed 2-stage guard band based algorithm is utilized in our DVB-T/H receiver system design. The hardware architecture of the first stage of the proposed integral CFO estimator is shown in Fig. 4.4. As we can see the signal power of the receiving data is calculated by two integral squarers instead of real multipliers to save the hardware implementation cost. The memory element is used to store the signal power of the l -th symbol and can be shared with the deinterleaver. Once the summation of the signal power within the left and right window is calculated, the comparator result can determine the shifted direction caused by integral CFO is positive or negative.

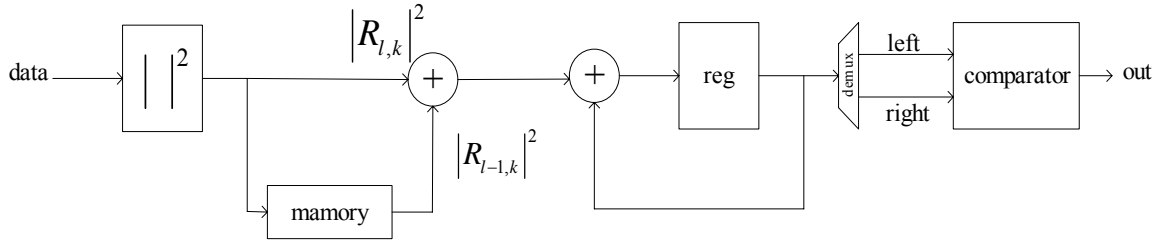


Fig. 4.4 Architecture of the first stage of the proposed integral CFO estimator

The hardware architecture of the second stage of the proposed integral CFO estimator is as shown in Fig. 4.5. As previous mentioned, two squarers are also exploited to calculate the signal power and can be shared with the first stage to save implementation cost. The signal power within search range of the $l-1$ -th and the $l-2$ -th symbol is stored in two memory elements that are shared with the deinterleaver. By the aid of a FIFO whose length is equal to the width of the moving window, the summation of signal power of the moving window can be obtained. An additional memory element is utilized for storing the summation of the signal power within the moving window in left-hand side of the guard band, and is also shared with the deinterleaver. Once the comparator detects the smallest summation value of signal power among the search range that is detected by the first stage, the corresponding index will be the estimated integral CFO value. The synthesis result of the proposed integral CFO estimator in a $0.18\mu\text{m}$ cell library with clock rate equals to 44MHz is shown in Table 4-2.

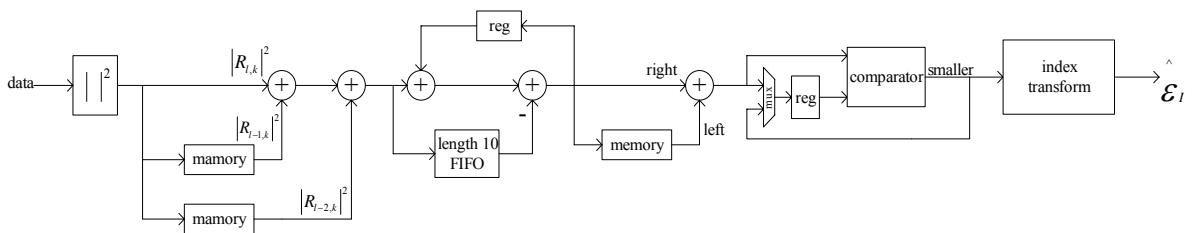


Fig. 4.5 Architecture of the second stage of the proposed integral CFO estimator

Table 4-2 Synthesis result of the integral CFO estimator

	Gate Count
Combinational	8955
Non-Combinational	2208
Total	11163

4.3.3 Residual Carrier Frequency Offset Tracking

The tracking stage of the proposed CFO synchronization scheme can be divided into two main blocks, the joint residual CFO/SCO estimator and the PI loop filter. The hardware architecture of the joint residual CFO/SCO estimator is shown in Fig. 4.6. As we can see the continual pilots of the previous symbol is stored in a memory element which is shared with the channel estimator. For the phase calculation, the joint CFO/SCO estimator also exploits the logarithm-based TLU arc-tangent method to achieve low power and high speed consideration. The architecture of the PI loop filter is already discussed in chapter 2 and as shown in Fig. 2.13. The synthesis result of the overall residual CFO tracking scheme in a $0.18\mu\text{m}$ cell library with clock rate equals to 44MHz is shown in Table 4-3.

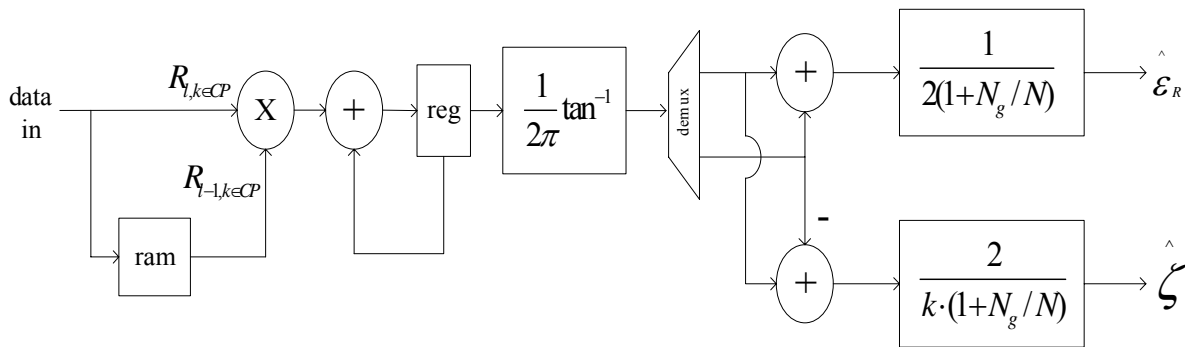


Fig. 4.6 Architecture of the joint residual CFO/SCO estimator

Table 4-3 Synthesis result of the residual CFO tracking scheme

	Gate Count
Combinational	11067
Non-Combinational	1269
Total	12336

4.4 DVB-T/H Baseband Receiver Chip Summary

Based on the proposed low complexity CFO synchronization scheme and other low power designs such as high speed FEC decoder and dynamic scheduling FFT processor [24], a DVB-T/H baseband receiver is implemented and taped out using 0.18um standard CMOS process in Jun. 2005. The layout view is shown in Fig. 4.7 with features listed in Table 4-4. The proposed baseband receiver contains 371.4K logic gates and 154.2Kbytes memory.

Table 4-4 Chip Feature

Technique	0.18um CMOS, 1P6M
Gate Count (Excluding SRAM)	371,353
Embedded Memory Size	154.2Kbytes
Package	208-pin CQFP
Core Size	6.9 X 5.8 mm ²
Clock Speed	109.7 MHz
Supply Voltage	1.8V Core, 3.3V I/O
Core Utilization	59.33%
Power Consumption at 31.67 Mbps	250 mW

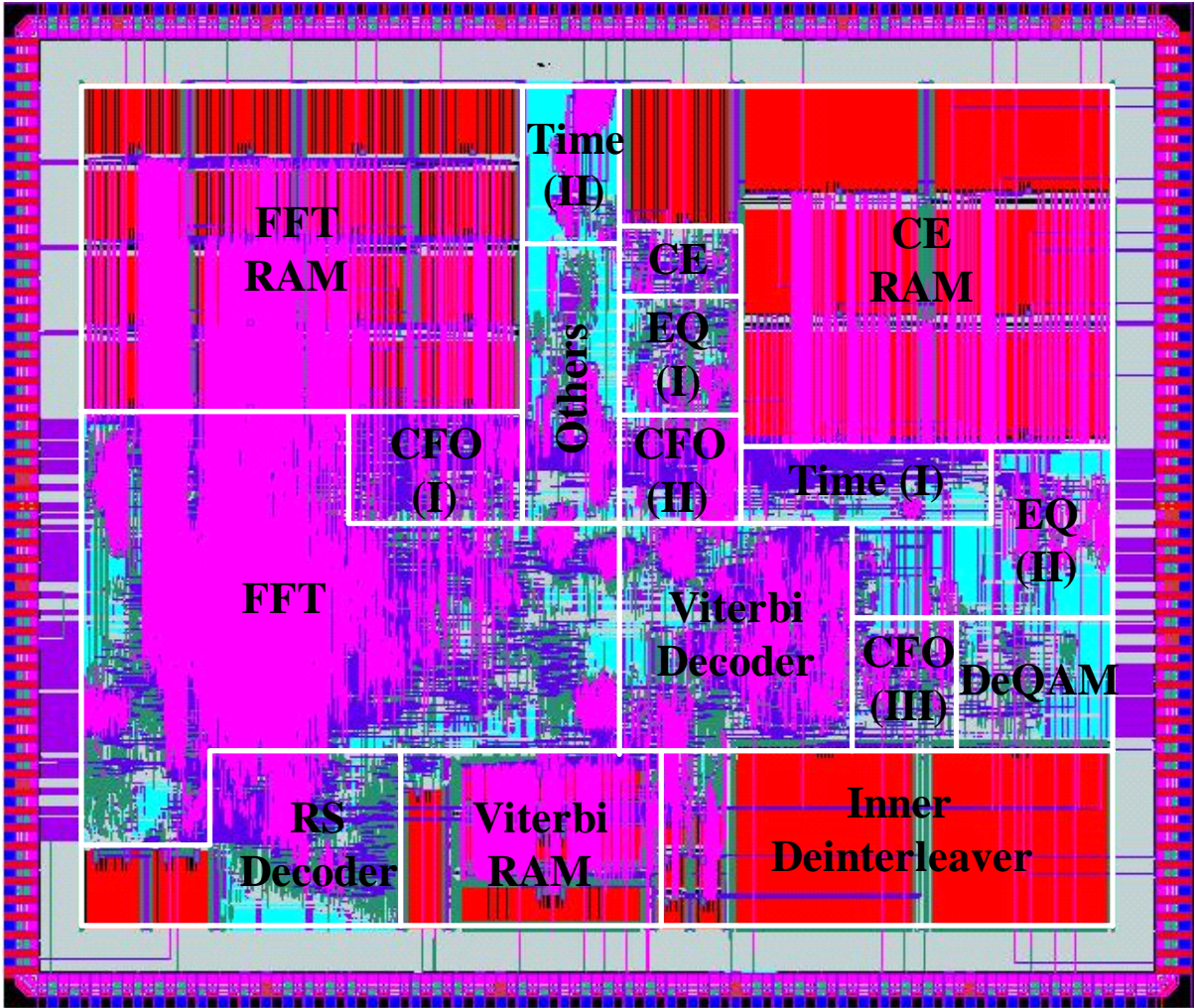


Fig. 4.7 Layout view of the DVB-T/H baseband receiver

Chapter 5 .

Conclusion and Future Work

After the algorithm illustration and performance analysis, the proposed low complexity CFO synchronization scheme is robust to solve CFO even in critical channel environment. In the proposed fractional CFO acquisition, the proposed algorithm can overcome the distortion within guard interval caused by multipath delay spread and achieves 0.25~7.8dB gain in RMSE compared with the conventional approach. In the proposed integral CFO acquisition, a 2-stage scheme is proposed to reduce the search range to about half of the conventional one. Besides, two low complexity algorithms are also proposed to detect the accurate integral CFO value and save more than 80% of number of multiplication without any performance loss to the overall system compared with the conventional approach. In the residual CFO tracking stage, the proposed three stage tracking loop can reduce the residual CFO error effectively. Applying the proposed CFO synchronization scheme, the synchronization loss to the overall DVB-T/H baseband receiver system is less than 0.2dB even in severe channel distortion including Rayleigh channel, Doppler spread 70Hz, CFO 92.14ppm (10.33 subcarrier spacing) and SCO 20ppm.

In this thesis, we focus on the synchronization with fixed CFO value in time-varying channel. For the future application with handheld terminals, the reception ability in mobile environment and limited operation power consumption will be the most important tasks. Therefore, a more robust synchronization scheme to time-varying CFO in severe mobile environment should be constructed. Furthermore, a fast and efficient CFO resynchronization scheme should be built to satisfy the low power issue in the future application.

Bibliography

- [1] Recharad Van Nee, and Ramjee Prasad, "OFDM for Wireless Multimedia Communications", pp.20-51, 2000.
- [2] Salzberg, B.R, "Performance of an Efficient Parallel Data Transmission System," *IEEE Trans. Comm.*, Vol. COM-15, pp.805-813, Dec. 1967.
- [3] ESTI EN 300 744 V1.5.1, "Digital Video Broadcasting (DVB); Framing Structure, Channel Coding and Modulation for Digital Terrestrial Television," Nov. 2004.
- [4] ESTI EN 300 401 V1.3.3, "Radio Broadcasting Systems; Digital Audio Broadcasting (DAB) to Mobile, Portable and Fixed Receivers," May 2001.
- [5] IEEE 802.11a IEEE Standards for Wireless LAN Medium Access Control and Physical Layer Specifications, Nov. 1999.
- [6] IEEE P802.15 Working Group, "Multi-band OFDM Physical Layer Proposal for IEEE 802.15 Task Group 3a," July 2003.
- [7] ESTI EN 302 304 V1.1.1, "Digital Video Broadcasting (DVB); Transmission System for Handheld Terminals (DVB-H)," Nov. 2004.
- [8] ETSI EN 301 192 V1.4.1, "Digital Video Broadcasting (DVB); DVB specification for Data Broadcasting," Nov. 2004.
- [9] P. H. Moose, "A Technique for Orthogonal Frequency Division Multiplexing Frequency Offset Correction," *IEEE Trans. Comm.*, Vol. 42, No. 10, pp. 2908-2914, Oct. 1994.
- [10] Hung-Kuo Wei, "A Frequency Estimation and Compensation Method for High Speed OFDM-based WLAN System," *MS Thesis, NCTU*, Jul. 2003.
- [11] J. J. van de Beek, et al., "A Time and Frequency Synchronization Scheme for Multiuser OFDM," *IEEE J. Select. Areas Comm.*, Vol. 17, No. 11, pp. 1900-1914, Nov. 1999.

- [12] M. Speth, S. Fechtel, G. Fock, and H. Meyr, "Optimum Receiver Design for OFDM-Based Broadband Transmission-Part II: A Case Study", *IEEE Trans. Comm.*, Vol. 49, No. 4, pp. 571-578, Apr. 2001.
- [13] D.-S. Han, J.-H. Seo, and J.-J. Kim, "Fast Carrier Frequency Offset Compensation in OFDM Systems," *IEEE Trans. Consumer Electronics*, Vol. 47, No.3, pp. 364-369, Aug. 2001.
- [14] P. Liu, B.-B. Li, Z.-Y. Lu, and F.-K. Gong, "A New Frequency Synchronization Scheme for OFDM," *IEEE Trans. Consumer Electronics*, Vol. 50, No.3, pp. 823-828, Aug. 2004.
- [15] D.-K. Kim, S.-H. Do, H.-K. Lee, and H.-J. Choi, "Performance Evaluation of the Frequency Detectors for Orthogonal Frequency Division Multiplexing," *IEEE Trans. Consumer Electronics*, Vol. 43, No.3, pp. 776-783, Aug. 1997.
- [16] Y.-J. Huang and S.-W. Wei, "Modified Guard Band Power Detection Methods for OFDM Frequency Offset Recovery," *IEEE Vehicular Technology Conf.*, Vol. 4, pp. 2277-2281, Oct. 2003.
- [17] M. Speth, S. Fechtel, G. Fock, and H. Meyr, "Optimum Receiver Design for Wireless Broad-Band Systems Using OFDM-Part I", *IEEE Trans. Comm.*, Vol. 47, No. 11, pp. 1668-1677, Nov. 1999.
- [18] S. Fechtel, "OFDM Carrier and Sampling Frequency Synchronization and Its Performance on Stationary and Mobile Channels", *IEEE Trans. Consumer Electronics*, Vol. 46, No.3, pp. 438-441, Aug. 2000.
- [19] Mingqi Li and Wenjun Zhang "A Novel Method of Carrier Frequency Offset Estimation for OFDM Systems", *IEEE Trans. Consumer Electronics*, Vol. 49, No.4, pp. 965-972, Nov. 2003.
- [20] Louis Litwin, "Matched Filtering and Timing Recovery in Digital Receivers," *RF design*, pp. 32-48, Sep. 2001.
- [21] Cheng-Wei Kuang, "Timing Synchronization for DVB-T System," *MS Thesis, NCTU*,

Sep. 2004.

- [22] P. Robertson and S. Kaiser, "The Effects of Doppler Spreads in OFDM(A) Mobile Radio Systems," *IEEE Vehicular Technology Conf.*, Vol. 1, pp. 329-333, Sep. 1999.
- [23] W. C. Jakes, "Microwave Mobile Communications," *John Wiley & Sons Inc.*, 1974.
- [24] Yu-Wei Lin, "The Matrix Prefetch Buffer Based FFT Processor," *MS Thesis, NCTU*, Jun. 2003.
- [25] Hsuan-Yu Liu, Yi-Hsin Yu, Chien-Jen Hung, Terng-Yin Hsu, Chen-Yi Lee "Combining Adaptive Smoothing and Decision-Directed Channel Estimation Schemes for OFDM WLAN Systems", *ISCAS*, 2003.
- [26] Yi-Hsin Yu, "A Channel Equalizer for OFDM-based Wireless Access Systems," *MS Thesis, NCTU*, Jun. 2004.

